Friction

Review Article

Molecular dynamics simulations addressing atomic-scale core issues in chemical mechanical polishing and post-CMP cleaning: A concise review

Lifei Zhang[1,✉], Ming Ji[2], Xinchun Lu[1,✉]

Cite this article: Zhang LF, Ji M, Lu XC. *Friction* 2026, **14**: 9441197. https://doi.org/10.26599/FRICT.2025.9441197

ABSTRACT: Chemical mechanical polishing (CMP) and post-CMP cleaning are critical steps in the current semiconductor manufacturing process. These processes require ensuring atomic-scale flatness and complete removal of contaminants. This review examines the use of molecular dynamics (MD) simulations to elucidate the atomic-scale mechanisms underlying CMP and postcleaning, focusing on four major MD methodologies: classical MD, reactive force field MD (ReaxFF), tight-binding quantum chemical MD (TB-QC MD), and ab initio MD (AIMD). Classical MD provides a foundation for simulating large-scale systems but lacks accuracy for modeling chemical reactions. ReaxFF allows real-time bond breaking and formation simulations during CMP. TB-QC MD combines quantum accuracy with classical efficiency, enabling exploration of the effects of chemical reactions on friction and material removal. AIMD directly calculates atomic interactions for precise depictions of chemical processes, although it is computationally expensive. MD simulations act as a "computational microscope", enhancing CMP and postcleaning processes by quantifying interactions, material removal pathways, and contaminant desorption. Future research should address multiscale modeling challenges, improve AIMD efficiency, and develop accurate potential functions to propel semiconductor manufacturing toward greater precision and efficiency.

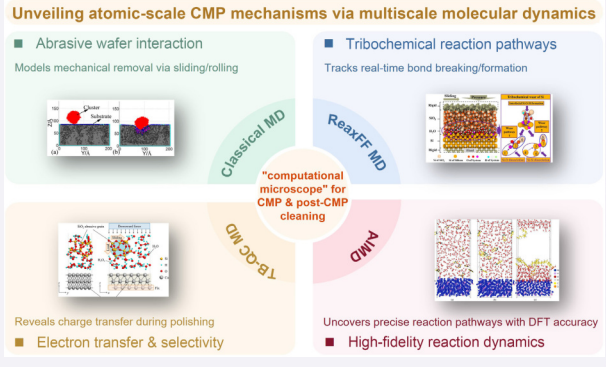

KEYWORDS: molecular dynamics (MD); chemical mechanical polishing (CMP); post-CMP cleaning; atomic scale; theory; tribochemistry

1 Introduction

1.1 CMP & post-CMP cleaning

The explosive growth of new fields such as AI, IoT, 5G, and smart manufacturing is demanding more integrated circuits. In response, the IC industry is relentlessly pursuing miniaturization while simultaneously increasing performance, ensuring reliability, and integrating more functions into a single chip [1–7], as shown in Fig. 1(a). As foundational components of modern technology, integrated circuits require chemical mechanical polishing (CMP) to fabricate complex 3D structures by ensuring atomic-scale layer flatness and interconnection integrity [6–10]. To extend the viability of Moore's law, essential efforts should concentrate on pioneering materials, breakthrough device structures, and cutting-edge fabrication techniques to further increase transistor integration levels [11–13]. Within this framework, CMP achieves nanometer-level global planarization through synergistic chemical-mechanical action, removing excess materials while providing ideal substrates for subsequent photolithography/-etching and increasing chip performance/yield [14–16]. This technique plays a vital role in three key aspects of advanced semiconductor manufacturing: the flattening of copper interconnect layers, the successful implementation of shallow trench isolation (STI) structures, and the integration of high-*k* dielectric materials within transistor gate architectures [17–20]. As process nodes advance below 3 nm, CMP proves indispensable in meeting exponentially escalating planarity demands [21–24]. However, the substantial chemical abrasives generated during the CMP process led to an exponential increase in contaminants, including nanoscale abrasive particles and reaction byproducts [17, 25–27]. These nanoparticles and chemically adsorbed layers form strongly bonded contaminants on nascent surfaces, which, if not thoroughly removed, can readily induce gate dielectric leakage

[1] State Key Laboratory of Tribology in Advanced Equipment, Tsinghua University, Beijing 100084, China. [2] Hwatsing Technology Co., Ltd., Tianjin 300350, China.
✉ Corresponding authors. E-mail: L. Zhang, lifeizhang@tsinghua.edu.cn; X. Lu, xclu@tsinghua.edu.cn

Received: August 29, 2025; Revised: October 21, 2025; Accepted: November 26, 2025

Nomenclature

ψ_i	The auxiliary parameter
$\dot{\psi}_i$	The KS orbitals
μ	Fictitious mass parameters
Ω	Volume
$\epsilon_{\alpha\beta}$	Strain
$\{\alpha_v\}$	External constraint parameters
ρ_ω	The wafer density
δ_{w}	The indentation depth of an abrasive particle into the wafer
χ	The volumetric concentration of abrasives in the slurry
γ	The proportion of the surface reverting to an unreacted state following the action of a subsequent abrasive particle
ρ_{s}	The density of the slurry prior to dilution
ρ_{a}	The density of the polishing particles
$\sigma_{\mathrm{asperity}}$	The arithmetic square root of the roughness on the wafer surface
δ_{aw}	The depth of particle embedding into the wafer surface
AIMD	Ab initio MD
A_{r}	The actual contact area between the pad and the wafer surface
A_{t}^*	The real-to-nominal contact area ratio
A_{t}	The apparent contact area between the pad and wafer
B_{ij}	The bond order
C	An empirical constant
C_0	The material removal attributed to chemical corrosion
CN	Coordination number
CPA	Contact–penetration–adhesion
CPMD	Car–Parrinello MD
CPUs	Central processing units
D	The mean abrasive diameter
DFT	Density functional theory
d_{m}	The nominal diameter of surface molecules
d	The contact area between abrasives and the wafer
d_{s}	The slurry dilution rate
E_{angle}	Energy associated with the valence angle strain (eV)
E_{bond}	Bond energy term (eV)
E_{Coulomb}	Coulomb interaction (eV)
E_{over}	Over coordination energy correction term (eV)
E_{s}	The Young's moduli of the abrasives
E_{specific}	System-specific terms (eV)
E_{system}	Total energy of the system (eV)
E_{tors}	Energy term related to the torsion angle (eV)
E_{total}	Total potential energy
E_{vdWaals}	Van der Waals interaction (eV)
E_{w}	The Young's moduli of the wafer
f_0	A unit-adjustment constant to ensure dimensional consistency
H_{p}	The hardness values of the pad
H_{w}	The hardness values of the wafer
GPUs	Graphics processing units
KS	Kohn-Sham
L	Lagrangian
M	The mass associated with the real degrees of freedom
m_i	The atomic weight of individual atoms
m_{s}	The slurry concentration before dilution
MC	Monte Carlo
MD	Molecular dynamics
MRR	Material removal rate
NEAIMD	Nonequilibrium ab initio molecular dynamics
N	The effective number of abrasive particles

(Continued)

Nomenclature	
P	The downforce
r_{ij}	The interatomic distance between atom i and atom j
R_{av}	The contact radius between the polishing particles and the wafer
ReaxFF	Reactive force field MD
R_{ij}	The distance between atoms i and j
R_I	The atomic coordinates
R_0, k, α, β	A fitting parameter
STI	Shallow trench isolation
SW	Stillinger–Weber
TB-QC MD	Tight-binding quantum chemical MD
TPU	Tensor processing unit
U_R	The repulsive potential terms
U_A	The attractive potential terms
$U_{Tersoff}$	The Tersoff potential
U	The potential term
$V_2(r_{ij})$	This function describes the potential energy between a pair of atoms (i and j)
$V_3(r_{ij}, r_{ik}, \theta_{ijk})$	The potential energy associated with the angular geometry of a triplet of atoms
v_i	The atomic velocity
V	The relative velocity between the pad and the platen
Vol_m	The volume of material removed per unit time by an individual abrasive
x_{avg}	The average diameter of the abrasives

through metal ion diffusion, increase contact resistance because organic residues block interconnect metal deposition, and degrade the process yield via particle-induced defects [22, 28–31]. Post-CMP cleaning therefore constitutes the critical process for eliminating polishing residues and ensuring device reliability, directly governing the precision limits of subsequent photolithography and thin-film processes while serving as the fundamental safeguard for sustaining Moore's Law advancement [21–33].

1.2 Factors of the CMP & post-CMP cleaning process

As shown in Fig. 1(b), the CMP process integrates three critical components: the polishing pad, slurry, and wafer carrier. The pad retains and distributes the abrasive slurry across the wafer-pad interface while providing conformability through surface topology, which directly influences the material removal rate (MRR) and within-wafer nonuniformity [8, 9, 34]. Slurry, a chemically reactive liquid medium, contains nanoscale abrasive particles [35] (typically silica particles), pH adjuvants [36, 37] (e.g., potassium hydroxide, ammonia), chelating agents [16, 26, 31, 38] (e.g., quinaldic acid), surfactants [7, 20, 39] (e.g., polyethylene glycol), and oxidants [40–46] (e.g., hydrogen peroxide, nitric acid), enabling the dual functions of surface chemical modification and mechanical removal of reacted layers. The wafer carrier holds the wafer while pressure is applied against the rotating polishing pad, which is fixed through a supported platform referred to as the platen platform [47–49]. The material is removed from the wafer surface as a result of mechanical abrasion by the pad and

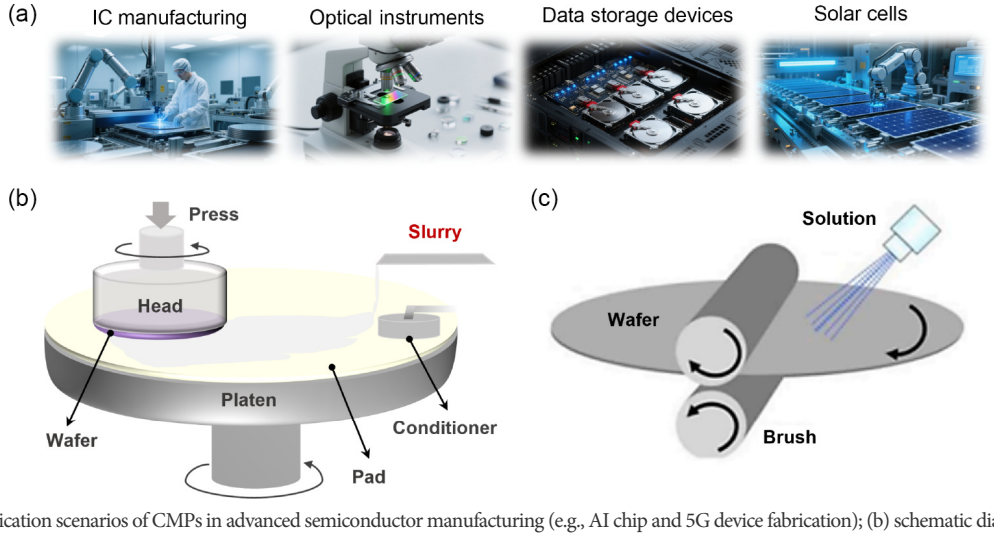

Fig. 1 (a) Key application scenarios of CMPs in advanced semiconductor manufacturing (e.g., AI chip and 5G device fabrication); (b) schematic diagram illustrating the core workflow of the CMP process (including slurry, pad, and wafer carrier interactions); (c) schematic of the post-CMP cleaning process.

abrasive particles, as well as chemical reactions with the slurry (polishing media), resulting in planarization [50, 51]. The process involves three key components: (1) mechanical action from the pad–slurry–wafer contact, (2) chemical modification of the surface layer by the slurry, and (3) subsequent mechanical removal of the chemically altered material, enabling controlled and uniform surface refinement at microscopic scales [52]. The MRR, uniformity, and surface integrity are critical metrics for evaluating machining performance and final workpiece quality [53–63]. Factors associated with wafer-pad interactions play pivotal roles in shaping polishing outcomes—particularly in achieving the atomic-scale planarization required for advanced semiconductor manufacturing [64]. The key contributing factors include three aspects: machine design (which determines the stability of wafer-pad contact), process parameters (such as downforce and kinematic settings that directly regulate polishing intensity [65]), and consumables (including slurries and polishing pads—critical for material removal efficiency [64]). These input parameters significantly affect various aspects of the wafer-pad interface, such as the pressure/stress profile on the wafer, consistency of the slurry film, relative sliding distance, and localized thermal fluctuations [64, 65]. Consequently, the final polishing results—such as surface flatness and process yield—stem from the combined effects of these interconnected parameters.

The post-CMP cleaning procedure is designed to remove residual impurities, including nanoscale particles, organic residues, and metallic ions [66–68]. The cleaning mechanism after CMP is complex, as the wafer surface achieves atomic-level roughness after polishing, leading to changes in its physical, chemical, and electrochemical properties [69–71]. Processes such as contaminant adsorption and desorption, as well as wafer corrosion, require special consideration [72]. During cleaning, it is crucial to ensure the removal of contaminants without introducing new contaminants or negatively impacting equipment performance. Cleaning methods in the semiconductor industry are generally classified into dry and wet cleaning methods [73]. Wet cleaning is the dominant approach for post-CMP cleaning, with common techniques including megasonic cleaning and mechanical brush cleaning [27, 74]. Megasonic cleaning uses high-frequency acoustic waves to disturb the solution, dislodging particles from the wafer surface, whereas mechanical brush cleaning involves rotating brushes and chemical liquids to remove contaminants [18, 29]. Mechanical brush cleaning is highly efficient, causes minimal surface damage, and is widely used, as shown in Fig. 1(c). The chemical action of the cleaning solution is also crucial, as it dissolves organic residues, etches thin films, and improves surface wettability, all while ensuring that it does not cause corrosion to the wafer or negatively impact the performance of low-*k* materials [75, 76].

1.3 Molecular dynamics

Nearly six decades ago, Anees Rahman released his pioneering computer simulation research focusing on the dynamics and motional correlations in liquid argon [77–79]—a work that marked the beginning of computer adoption in physical–chemical research, laying the foundational groundwork for subsequent molecular dynamics (MD) applications in fields such as CMPs. The multiscale system analysis shown in Fig. 2 employs scale-specific methodologies, including macroscopic finite element modeling, calculation of phase diagrams, atomic-scale MD, mesoscopic Monte Carlo (MC) simulations, and quantum-level first-principles density functional theory [80–84]. Quantum approaches provide precise descriptions of electronic structures and reaction mechanisms at surfaces; however, the extreme computational demands limit their application to systems of only approximately 100 atoms and picosecond durations—far below what is needed to investigate tribological mechanisms or experimentally observable processes. MD overcomes the limitations of traditional methods by leveraging quantum-parameterized force fields to simulate millions of atoms over nanosecond durations [85, 86]. By solving Newtonian equations of motion, MD provides unique insights into time-dependent chemical-mechanical synergies, atomic-scale thermodynamics, structural evolution, transport mechanisms, and mechanical responses—capabilities that exceed the MC's statistical averaging approach. As a powerful computational tool, MD acts as a "computational microscope", enabling detailed investigations of MDs and their interactions with the environment at the atomic level—an achievement that is difficult to achieve with most experimental techniques. On the basis of classical mechanics, MD simulates a molecular system's dynamic behavior by numerically solving the Newtonian equation of motion for each molecule. In MD simulations, the force field plays an essential role in determining the interatomic potentials and physical behaviors of particles, encompassing van der Waals forces and electrostatic interactions, among other types [87, 88]. While MD simulations demand significant computational resources and rely on the accuracy of force field parameters, their importance and value in scientific research are undeniable.

A wide range of parallel MD packages have been developed and are supported by extensive user communities. Prominent examples designed for biomolecular simulations include AMBER [89], CHARMM [90], GROMACS [91], and NAMD [92], whereas software such as DL_POLY [93], GULP [94], HOOMD-blue [17], and LAMMPS [23] are employed primarily in materials modeling. Most of these packages are distributed under open-source licenses and are optimized for parallel computing across both graphics processing units (GPUs) and central processing units (CPUs), enabling high-performance simulations across multiple time and length scales.

On the basis of potential function accuracy and computational efficiency, mainstream MD methods fall into four categories. A comprehensive comparison of the specific properties is provided in Table 1.

Classical MD is a simulation method based on Newtonian mechanics. The core idea is to treat atoms as classical particles and describe their motion trajectories by solving Newton's equations

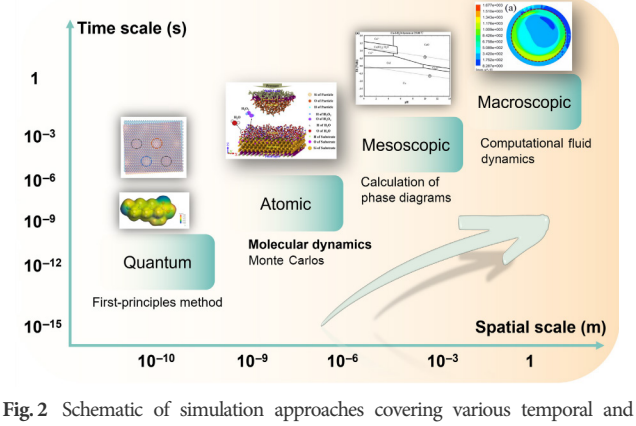

Fig. 2 Schematic of simulation approaches covering various temporal and spatial scales—including those applied to MD studies for CMP. Reproduced with permission from Ref. [31], © Elsevier B.V. 2023; Ref. [43], © Elsevier B.V. 2017; Ref. [97], © Elsevier B.V. 2015; Ref. [95], © The Author(s) 2022; Ref. [96], © Taylor & Francis Group, LLC 2021.

Table 1 Accuracy–efficiency trade-offs in classical MD, ReaxFF MD, TB-QC MD, and AIMD

Method category	Classical MD	ReaxFF MD	TB-QC MD	AIMD/CPMD
Potential energy basis	Pure empirical potentials	Empirical + dynamic bond order	Semiempirical QM	First principles
Electronic structure handling	None	Dynamic charges	Approximate explicit	Explicit solution
Simulates chemical reaction	No	Yes	Yes	Yes
Parametrization required	High	High	High	Minimal
Computational complexity	$O(N)/O(N\log N)$	$O(N^2)$	$O(N^2)/O(N^3)$	$O(N^2)$
Typical system size	> 1,000,000 atoms	1,000–100,000 atoms	100–10,000 atoms	10–1,000 atoms
Typical time scale	μs–ms	ns–100 ns	ps–ns	< 100 ps
Key strength	Fast, large systems	Reactive, moderate scale	Electronic structure, faster than AIMD	Highest accuracy, universal
Primary limitation	No reactivity, no electronics	Parametric, limited accuracy	Parametric, less accurate than AIMD	Extremely expensive, small/short
Typical application	Biomolecules, material mechanics	Combustion, fracture, and damage	Defects, nanoelectronics	Precise reaction mechanisms, electronics

of motion [98, 99]. In classical MD, atomic interactions are typically described via predefined force field models (such as force field parameters), which include terms such as bond energy, angles, and van der Waals forces. Classical MD utilizes purely empirical potentials such as harmonic oscillators and Lennard–Jones functions with fixed bond parameters for nonreactive systems. Its $O(N)$-scale efficiency enables simulations of million-atom biomolecular folding and material mechanics at microsecond-to-millisecond timescales, although it cannot capture electronic structures or chemical reactions [100]. Classical MD is widely used in fields such as materials science and biochemistry, but its limitations include the need for numerous empirical parameters and difficulty in handling complex chemical reaction processes.

Reactive force field MD (ReaxFF MD) is a simulation method that combines classical mechanics with quantum mechanics concepts [101]. Its core idea is to describe atomic interactions through a force field model while allowing bond breaking and formation. ReaxFF MD incorporates dynamic bond orders to model bond breaking/formation, handling combustion and polymer fracture in 1,000–100,000 atom systems at nanosecond scales but remains parametrically empirical with limited accuracy [102]. Unlike traditional classical MD, ReaxFF MD can simulate chemical reactions, such as bond formation and cleavage, offering a more accurate representation of chemical processes [103].

Tight-binding quantum chemical MD (TB-QC MD) is a multiscale modeling approach that integrates quantum-mechanical accuracy with the computational efficiency of classical methods [104]. The core idea is to use quantum mechanical methods to calculate electronic structures and classical mechanics to handle the motion of atomic nuclei. TB-QC MD employs semiempirical quantum approximations via tight-binding methods to compute electronic structures through simplified Hamiltonians, simulating semiconductor defects and nanomaterial electronics in 100–10,000 atom systems at ps–ns timescales with $O(N^3)$ complexity. This method provides high computational accuracy when dealing with complex systems but has high computational costs. This method is predominantly used for simulating systems at reduced scales.

Ab initio molecular dynamics (AIMD) is a first-principles quantum mechanics-based method [105]. Its core idea is to directly calculate atomic interactions via quantum chemistry methods (such as density functional theory) without requiring predefined force field parameters [106]. AIMD leverages density functional theory or the Hartree–Fock equation to solve electronic ground-state wave functions, accurately modeling catalytic pathways and proton transfer in sub100-atom systems below 100 ps timescales, while increasing $O(N^3)$ costs three orders of magnitude greater than those of classical methods. AIMD enables precise modeling of chemical phenomena—including bond dissociation and formation—thereby offering significant value for research in catalysis, materials science, and related disciplines.

These approaches form an accuracy–efficiency spectrum: accuracy ranks as classical MD < ReaxFF < TB-QC MD < AIMD, whereas computational cost increases inversely [107]. Selection follows triage criteria—reaction necessity, system size, and precision demands: classical fields for nonreactive large systems; ReaxFF for reactive mesoscale systems; TB-QC MD when electronic properties are essential; and AIMD for ultrahigh-precision small-scale investigations [108, 109]. The strategic application of these multiscale MD methods is poised to address the fundamental challenges in CMP and post-CMP cleaning, particularly as process nodes advance to 3 nm and beyond. When experimental techniques struggle to probe the atomistic mechanisms at the wafer–abrasive–slurry interface, MD simulations serve as a powerful "computational microscope". They bridge the critical gap between macroscopic process parameters and atomic-level phenomena. For example, AIMD can elucidate the initial bond-breaking pathways and catalytic role of oxidizers with quantum accuracy; ReaxFF MD can simulate the entire process of interface bridging bond formation and material removal across thousands of atoms; TB-QC MD offers a balanced view of charge transfer during tribochemical reactions; and classical MD can model the adsorption and desorption dynamics of contaminants and surfactants during cleaning over relevant timescales. This review aims to systematically consolidate how these MD techniques, each with their unique strengths, collectively provide a foundational atomic-scale framework. By deciphering the chemical–mechanical synergy, they guide the rational design of slurries, optimization of process parameters, and development of effective cleaning strategies, ultimately contributing to the achievement of the atomic-scale planarization and contamination-free surfaces required for next-generation semiconductor manufacturing.

1.4 Selection and application of potential functions

ReaxFF MD. ReaxFF is a reactive force field proposed by van Duin et al. [110] to describe the breakage and formation of bonds. The components of the ReaxFF potential energy are detailed as Eq. (1) [6]:

$$E_{\text{system}} = E_{\text{bond}} + E_{\text{over}} + E_{\text{angle}} + E_{\text{tors}} + E_{\text{vdWaals}} + E_{\text{Coulomb}} + E_{\text{specific}} \quad (1)$$

where nonbonded interactions include long-range Coulombic contributions (E_{Coulomb}) and short-range van der Waals dispersive forces (E_{vdWaals}), which are computed universally across all atomic pairs irrespective of connectivity. The detailed expression of each potential component is shown in Ref. [111].

The Stillinger–Weber (SW) potential [112] is an empirical interatomic potential that combines two- and three-body interactions. It was initially developed for covalent solids such as silicon. However, much like the Tersoff potential, the SW potential is also unsuitable for modeling systems where chemical reactions occur. The expression for the total potential energy is given as Eq. (2):

$$E_{\text{total}} = \sum_{i<j} V_2(r_{ij}) + \sum_{i<j<k} V_3(r_{ij}, r_{ik}, \theta_{ijk}) \quad (2)$$

where $V_2(r_{ij})$ and $V_3(r_{ij}, r_{ik}, \theta_{ijk})$ are the two-body and three-body terms, respectively. They are dependent on the distance between two atoms and the angle between three atoms. The SW potential is appropriate for simulating bond formation and dissociation processes associated with grain growth, fracture, dislocation dynamics, nanoindentation, etc.

TB-QC MD. The total energy within the TB-QC MD framework [46] is computed as Eq. (3):

$$E = \sum_{i=1}^{N} \frac{1}{2} m_i v_i^2 + \sum_{k}^{\text{OCC}} \varepsilon_k + \sum_{i=1}^{N} \sum_{j>i}^{N} \frac{Z_i Z_j}{R_{ij}} + \sum_{i=1}^{N} \sum_{j>i}^{N} E_{ij}^{\text{repul}}(R_{ij}) \quad (3)$$

where

$$E_{ij}^{\text{repul}}(R_{ij}) = f_0 b_{ij} \exp\left(\frac{a_{ij} - R_{ij}}{b_{ij}}\right) \quad (4)$$

Within these equations, m_i denotes the atomic weight of individual atoms, whereas v_i represents the atomic velocity—both parameters play an essential role in characterizing the dynamical properties of the molecular system. ε_k corresponds to the eigenvalue of the kth occupied molecular orbital, which reflects the electronic energy state of the system [9]. For Z_i and Z_j, these are Mulliken atomic charges derived from single H diagonalization, a common method for charge distribution calculation in MD simulations [46]. Additionally, f_0 serves as a unit adjustment constant to ensure dimensional consistency, and R_{ij} represents the distance between atoms i and j. Parameters a_{ij} and b_{ij} correlate with the atomic size and stiffness in that order, directly influencing the accuracy of interatomic interaction modeling [9].

The Tersoff potential was first proposed for covalent solids [113], where the bond order and bond angle are the dominant characteristics. The strength of the bond between two atoms depends on their local atomic arrangement, especially the coordination number and bond angle. The developed Tersoff potential is represented by the general expression in Eq. (5):

$$U_{\text{Tersoff}} = \frac{1}{2} \sum_{i \neq j} U_{\text{R}}(r_{ij}) + \frac{1}{2} \sum_{i \neq j} B_{ij} U_{\text{A}}(r_{ij}) \quad (5)$$

where U_{R} and U_{A} represent the repulsive and attractive potential terms, respectively, and where r_{ij} denotes the interatomic distance between atom i and atom j. The bond order B_{ij} generally tends to decrease with increasing coordination number.

AIMD. The fundamental concept underlying AIMD [114] is to reformulate the minimization of the Kohn–Sham (KS) energy functional—which corresponds to determining the ground-state electronic structure—as a dynamical evolution within an extended classical Hamiltonian framework. In this system, not only are the atomic coordinates R_I treated as dynamical variables, but the KS single-particle orbital wave functions $\psi_i(r)$ that describe the electronic states are also considered time-dependent classical fields, assigned fictitious mass parameters μ. Additionally, possible external constraint parameters $\{\alpha_v\}$ of the system (such as volume Ω and strain $\epsilon_{\alpha\beta}$) can also be treated as dynamical variables and assigned fictitious masses μ_v. The system's time evolution is governed by an extended Lagrangian of the form:

$$L = \sum_i \mu \int_\Omega \mathrm{d}^3 r |\dot{\psi}_i|^2 + \sum_I \frac{1}{2} M_I \dot{R}_I^2 + \sum_v \frac{1}{2} \mu_v \dot{\alpha}_v^2 - E[\{\psi_i\}, \{R_I\}, \{\alpha_v\}] \quad (6)$$

where $\dot{\psi}_i$ represents the KS orbitals; M represents the mass associated with the real degrees of freedom; ψ_i is the auxiliary parameter related to the fictitious dynamics; and R_I denotes the atomic coordinates, which are treated as dynamical variables. The energy E associated with $\{\psi_i\}$ and $\{R_I\}$ is described by the KS energy functional, which depends on the functions $\{\psi_i\}$, the atomic coordinates $\{R_I\}$, and other components. Its form is typically standard in density functional theory (DFT).

$$E = \sum_i \int_\Omega \mathrm{d}^3 r \psi_i^*(r) \left(-\frac{\hbar^2}{2m} \nabla^2\right) \psi_i(r) + U[n(r), \{R_I\}, \{\alpha_v\}] \quad (7)$$

In this formulation, the potential term U encompasses the Coulombic ion–ion repulsion, the external pseudopotential contribution, the Hartree energy, and the exchange–correlation energy. The electron density is expressed as $n(r) = \sum_i |\psi_i(r)|^2$.

Constraints: The KS orbitals must always remain orthonormal.

$$\int_\Omega \mathrm{d}^3 r \psi_i^*(\boldsymbol{r}, t) \psi_j(\boldsymbol{r}, t) = \delta_{ij} (\text{holonomic constraints}) \quad (8)$$

The ReaxFF reactive force field encompasses all main-group and transition-metal elements, making it applicable to systems that exhibit diverse reactive processes, including bond formation and cleavage, polarization effects, and charge transfer. Car–Parrinello MD (CPMD) is a kind of AIMD and is applicable for systems involving changes in electronic structure, such as metals, semiconductors, insulators, etc. CPMD enables the investigation of electronic transfer mechanisms, bond dissociation and formation dynamics in chemical reactions, along with electronic properties such as band structure, density of states, and charge distribution. TB-QC MD is mainly used to study complex processes involving chemical bond breakage and formation and strikes an effective compromise between computational cost and predictive precision. However, it is faster than CPMD. The Tersoff potential function is used mainly for covalently bonded substances, such as group IV elements (C, Si, and Ge) and their compounds. It is specifically designed for tetrahedral materials, with the most famous and successful application being Si. Its core lies in stabilizing specific bond angles (especially the tetrahedral angle of 109.47°) by introducing explicit three-body interaction terms, which are crucial for describing materials with diamond or zinc blende structures. The SW potential is mainly used for two-dimensional materials, such as molybdenum disulfide and graphene, and can accurately reflect the dual characteristics of intralayer covalent bonds and interlayer van der Waals forces in layered materials.

1.5 Highlights in this paper

In recent years, several review articles have focused on specific aspects of CMPs, such as theoretical models [64], CMP techniques for different substrates [17, 34], the achievements and limitations of classical MD [4], the application of MD in tribology [39, 115], the development and application of ReaxFF MD [6, 7], and the use of machine learning to assist CMPs [5], among others. However, to the best of our knowledge, no prior study has comprehensively reviewed the application of MD in both CMP and post-CMP cleaning processes. Additionally, the mechanisms of mechanical, chemical, and synergistic effects at the atomic level during CMP processes have received limited attention. To address this research void, the present study surveys major classes of MD methods and examines their respective applications in the CMP and post-CMP cleaning processes.

2 The incorporation of MD into CMP & post-CMP cleaning optimization

2.1 Applying classic MD to CMP & post-CMP cleaning

To enhance the regulation of MRR during CMP, an empirical model has been developed from historical experimental results, alongside a mathematically formulated MRR model grounded in mechanical and statistical principles. Equation (9), the Preston equation [53], is one of the earliest models and is widely applied. This model reflects only the effects of the mechanical pressure and relative velocity on material removal.

$$\mathrm{MRR} = kPV \tag{9}$$

In Eq. (9), P represents the downforce in the polishing process, V represents the relative velocity between the pad and the platen, and k is a coefficient related to other variables. Since the experimental results from CMP do not fully comply with the Preston equation, other mathematical models [54–63] have been proposed to describe the corresponding experimental phenomena.

The generation and subsequent elimination of the surface film represent a dynamically evolving process that is critically affected by the MRR, planarity uniformity, and chemical selectivity of the slurry [50, 51]. In particular, during the polishing of metals and oxides, chemical reactions significantly affect the surface dissolution rate. Maury et al. [54] demonstrated through experiments that under higher pressures, a constant term may be incorporated into the Preston equation (Eq. (10)) to improve its agreement with experimental observations.

$$\mathrm{MRR} = kPV + R_0 \tag{10}$$

In Eq. (10), R_0 is a fitting parameter whose value can be determined through linear regression of the experimental results. In the above mathematical models, the MRR has a linear relationship with velocity and pressure, but many experimental results suggest that using nonlinear mathematical models can better describe the experimental phenomena, as shown in Eq. (11).

$$\mathrm{MRR} = kP^{\alpha}V^{\beta} \tag{11}$$

In Eq. (11), k, α, and β can be fitted from experimental data. On the basis of experimental data, Tseng and Wang [55] derived a model suitable for oxide polishing with α = 5/6 and β = 1/2, whereas Shi and Zhao [56] developed a modeling approach for soft pads (which are softer than the particles and wafer) with α = 2/3 and β = 1.

The above models do not account for other factors that affect material removal, such as the wafer, pad, abrasives, and slurry. To consider as many of these factors as possible, researchers have developed more complex models by combining theoretical and experimental methods. On the basis of principles of statistics and elasticity theory, Liu et al. [57] incorporated mechanical properties—including the hardness and Young's modulus of the wafer, polishing pad, and abrasive particles—to develop a mathematical model, presented in Eq. (12).

$$\mathrm{MRR} = C\left(\frac{H_{\mathrm{w}}}{H_{\mathrm{w}}+H_{\mathrm{p}}}\right)\left(\frac{E_{\mathrm{s}}+E_{\mathrm{w}}}{E_{\mathrm{s}}E_{\mathrm{w}}}\right)PV \tag{12}$$

In Eq. (12), H_{w} and H_{p} denote the hardness values of the wafer and pad, respectively; E_{s} and E_{w} are the Young's moduli of the abrasives and the wafer, respectively; and C is an empirical constant incorporating the effects of additional influencing factors.

Building on contact mechanics and statistical theory, Luo and Dornfeld [58] introduced a material removal model, which is given in Eq. (13).

$$\mathrm{MRR} = \rho_{\omega}N\left(\overline{Vol}\right)_{\mathrm{m}} + C_0 \tag{13}$$

In Eq. (13), ρ_{ω} represents the wafer density, N represents the effective number of abrasive particles, Vol_{m} represents the volume of material removed per unit time by an individual abrasive, and C_0 represents the material removal attributed to chemical corrosion. This model comprehensively considers factors such as the number of effective abrasives, abrasive size distribution, pad hardness, pad roughness, wafer hardness, and velocity and pressure parameters. This model is founded upon the following fundamental assumptions: (1) the influence of fluid on the wafer surface is negligible; (2) interactions among the polishing pad, wafer, and abrasive particles occur through solid-solid contact; (3) the asperities on the rough surface are spherical and possess identical radii of curvature; (4) surface asperities are uniformly distributed with a constant areal density; (5) the deformation behavior between the wafer and particles, as well as between the pad and abrasives, is purely elastic; and (6) the abrasive particle sizes conform to a normal distribution.

Drawing on elastoplastic contact mechanics and abrasive wear mechanisms, Zhao and Chang [59] developed a mathematical model (Eq. (14)) that incorporates the synergistic effects of chemical and mechanical factors during material removal.

$$\mathrm{MRR} = \alpha\frac{9.9}{\pi^{5/3}}VA_{\mathrm{t}}^{*}\left(\frac{\delta_{\mathrm{w}}}{D}\right)^{2}\chi^{2/3} \tag{14}$$

In Eq. (14), α denotes the density ratio between the chemically reacted surface layer and the bulk wafer material, A_{t}^{*} represents the real–nominal contact area ratio, δ_{w} indicates the indentation depth of an abrasive particle into the wafer, D corresponds to the mean abrasive diameter, and χ signifies the volumetric concentration of abrasives in the slurry. The real contact area is derived from the Greenwood–Williamson elastic contact model; the effective number of particles is calculated on the basis of the total pad–wafer contact area and the abrasive concentration; and the particle indentation depth is obtained by solving the force balance equations applied to abrasives during wear, in conjunction with principles of contact mechanics.

Furthermore, Zhao et al. [60] proposed that chemical reactions transform strongly bonded surface atoms/molecules into weakly bonded species, whereas mechanical interactions facilitate the fracture of these weakened bonds, thereby enabling material removal. Their derived model is presented in Eq. (15).

$$V = \frac{\pi d_m u d A_t}{6\left[(1/\beta)+(1/\gamma)-1\right]}\left(\frac{6\chi}{\pi D^3}\right)^{2/3} \quad (15)$$

In Eq. (15), V refers to the volumetric removal rate of the wafer material, d_m denotes the nominal diameter of surface molecules, d represents the contact area between abrasives and the wafer, u is the coefficient of friction, A_t indicates the apparent contact area between the pad and wafer, D represents the mean abrasive diameter, χ corresponds to the volumetric abrasive concentration in the slurry, β signifies the fraction of chemical reactions occurring at contact sites within the time interval between two consecutive abrasive interactions, and γ reflects the proportion of the surface reverting to an unreacted state following the action of a subsequent abrasive particle.

Unlike the assumption of elastic contact deformation by Luo et al., Jeng and Wang [61] and Jeng and Huang [62] proposed that the contact between rough peaks is elliptical and developed an elastoplastic contact model. On the basis of this model, they established a material removal model, as shown in Eq. (16).

$$\mathrm{MRR} = \frac{d_s \cdot \rho_s \cdot m_s}{\rho_a \cdot \frac{\pi}{6} \cdot x_{avg}^3} \cdot A_r \cdot (3 \cdot \sigma_{asperity} - d) \cdot \delta_{aw} \cdot R_{av} \cdot V \quad (16)$$

In Eq. (16), R_{av} represents the contact radius between the polishing particles and the wafer, and d_s denotes the slurry dilution rate. For the slurry-rated parameters, ρ_s represents the density of the slurry prior to dilution, and m_s represents the slurry concentration before dilution. Additionally, ρ_a is the density of the polishing particles, x_{avg} refers to the average diameter of the abrasives, and A_r signifies the actual contact area between the pad and the wafer surface. Other key variables included the distance between the wafer and pad surfaces after pressure equilibrium, $\sigma_{asperity}$ (the arithmetic square root of the roughness on the wafer surface), δ_{aw} (the depth of particle embedding into the wafer surface), and v (the relative velocity in the polishing process) [61, 62].

Wang et al. [63] considered the promoting effect of polishing pressure on chemical reactions and established the model shown in Eq. (17).

$$\mathrm{MRR} = \left[\frac{V_P D_0}{2r_c} e^{-\frac{1}{2}(1-2\nu_1)(P_s + C f_b E_1/10)\Delta V_d / R_0 T}\right]^{1/2} \quad (17)$$

Equation (17) suggests that the MRR depends on the abrasive size, polishing parameters, and elastic moduli of both the abrasive particles and the wafer substrate.

The above mathematical models can predict the MRR to a certain extent during the CMP process, thus providing a basis for controlling the process, such as adjusting parameters such as the polishing speed and pressure. The progression from the Preston equation to the more sophisticated models (Eqs. (12)–(17)) reflects a concerted effort to capture the complex, multiphysics nature of a CMP.

Model progression and focus: The models evolve from purely empirical (Eqs. (10) and (11)) to those grounded in specific physical theories. Liu's model (Eq. (12)) incorporates the mechanical properties of the wafer, pad, and abrasive, making it particularly relevant for understanding the role of material hardness and stiffness in polishing, especially for oxide CMPs. Luo's model (Eq. (13)) represents a significant leap by explicitly introducing statistical concepts and, crucially, separating the chemical contribution (C_0).

The advent of chemomechanical synergy: The later models explicitly aim to quantify the celebrated chemical-mechanical synergy. Zhao's models (Eqs. (14) and (15)) are pioneering in this regard. Equation (14) links the MRR to the indentation depth of abrasives and the properties of a chemically softened surface layer (α), making it powerful for scenarios where surface modification is key. Equation (15) further introduces kinetic parameters (β, γ) that describe the surface reaction and repassivation cycle, offering a more dynamic view of the chemical–mechanical interaction.

Refining contact mechanics: Jeng and Wang's model (Eq. (16)) challenges the assumption of purely elastic contact and spherical asperities, offering a more realistic elastoplastic contact model. This makes it advantageous for situations involving softer pads or wafers where plastic deformation is significant. Finally, Wang's pressure-dependent kinetic model (Eq. (17)) uniquely accounts for the direct promotion of chemical reaction rates by mechanical pressure.

In summary, the choice of model depends on the specific CMP context: for a first-order estimate dominated by mechanics, the extended Preston equations suffice; for a breakdown of mechanical property influences, models such as Eqs. (12) and (16) are appropriate; and for a deep dive into the chemical–mechanical interplay, the models by Zhao and Wang (Eqs. (14), (15), and (17)) provide the most granular insight. Collectively, they represent a toolbox of increasing sophistication, each built upon the physical insights of its predecessors to decouple and quantify the myriad factors governing material removal.

However, since material removal occurs at the micro/nanoscale, these models cannot accurately describe the microscopic mechanisms of material removal. Therefore, new methods for conducting in-depth exploration of the material removal mechanisms at the microscopic level during CMP are needed. MD simulation offers a suitable approach for addressing this type of problem. While these mathematical models are powerful for process prediction, many of their core parameters, such as the contact area and chemical–mechanical synergy, remain idealized. MD simulations address this gap by enabling direct atomic-scale observations of these very phenomena. MD can quantify key model parameters and validate their underlying assumptions—for example, by directly measuring the depth of abrasive indentation or visualizing the removal of a chemically weakened layer—thus providing a critical physical foundation for the analytical frameworks and guiding their refinement.

During CMP, material removal primarily occurs through the rolling and sliding of abrasives. Beyond the impact of process parameters, the role of the heterogeneous surface layer on the wafer warrants further examination.

Sliding. MD simulations are extensively employed to investigate the material removal mechanisms of substrate surfaces subjected to impacts from large porous clusters with diverse pore size distributions. As shown in Fig. 3(a), Chen et al. [116, 117] simulated the mechanical collision process of silica clusters with silicon substrates in both dry and water-containing environments. The findings from their study—visualized in Figs. 3(b) and 3(c)—demonstrated that under otherwise identical conditions, the substrate sustains more significant damage from solid silica cluster impacts than from porous silica cluster impacts; additionally, the severity of such damage progressively decreases with increasing pore diameter within the porous clusters [116, 117]. This observation provides a microscopic basis for understanding abrasive–pad interaction effects in CMPs, where porous abrasives are often preferred for reducing substrate damage. During collision, silicon protrusions can form on the silicon surface due to thermal diffusion, phase transformation, and lattice slip at the collision interface. Shi et al. [118] simulated the nanoscratching

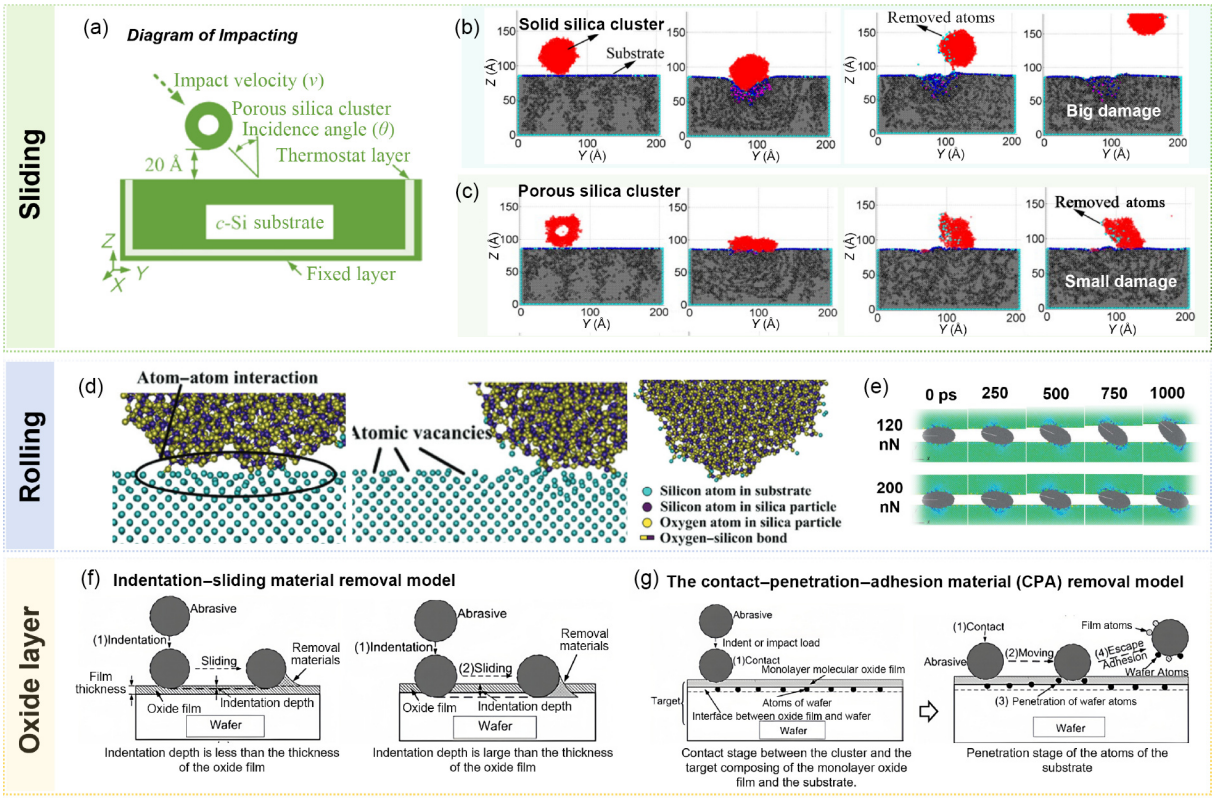

Fig. 3 Sliding-induced impact: (a) schematic illustration of silica clusters impacting a crystalline silicon substrate—corresponding to sliding-related abrasive-substrate interaction mechanisms in CMP; (b, c) cross-sectional side views of the impact zone at different time points: (b) solid silica cluster impact, (c) porous silica cluster impact. Rolling-induced material removal: (d) material removal features during the abrasive rolling process, highlighting interfacial atomic interactions between the silicon substrate and silica particles, the formation of atomic vacancies on the substrate after particle passage, and the structural configuration of the abrasive particle following traversal; (e) instantaneous atomic configurations under varying normal loads—reflecting how load affects abrasive rolling behavior in a CMP. Oxide layer-regulated removal models: (f) schematic illustrations of the indentation–sliding material removal model applied in CMP processes; (g) schematic illustrations of the CPA (contact–penetration–adhesion) removal model for CMP processes—critical for interpreting oxide layer-mediated material removal mechanisms. Reproduced with permission from Ref. [117] for (a–c), © Elsevier B.V. 2012; Ref. [122] for (d), © American Institute of Physics 2011; Ref. [127] for (e), © The Royal Society of Chemistry 2017; Ref. [126] for (g), © Elsevier B.V. 2014.

behavior of monocrystalline Cu with varying water film thicknesses during the CMP process and revealed that the water film exerts dual effects on the interfacial friction: it increases the friction force acting on the abrasive particle due to the resistance of water accumulated ahead of the particle, but reduces the friction force on the Cu surface through lubrication. They also found that the accumulation of water molecules around the particle induces anisotropic ridge formation, surface damage around the groove, and irregular groove structures, and the material removal efficiency decreases significantly with increasing water film thickness. Notably, they emphasized that an appropriate rather than ultra-high removal efficiency should be prioritized in real CMP processes to achieve defect-free, high-quality polished surfaces. Ye et al. [119] conducted MD simulations of Cu surface polishing at the nanoscale, incorporating the synergistic contributions of mechanical and chemical interactions. Their study revealed that mechanical sliding of surface particles caused dislocations on the Cu surface, whereas chemical actions reduced friction during sliding, preventing dislocation formation and resulting in a smoother polished surface. The model accounted for chemical effects by ensuring that Cu atoms, whose potential energy exceeded a specific threshold, no longer interacted with the substrate but were chemically dissolved, with the threshold adjusted to control the intensity of the chemical interactions. Dai et al. [120] simulated the interaction between silica particles and silica surfaces and reported that the geometry of surface roughness peaks significantly influenced material removal, whereas the relative sliding speed had a lesser effect. During sliding, deformed rough peaks caused a greater increase in temperature, and the material was transferred from the particles to the substrate, resulting in a smoother surface. Han et al. [121] subsequently used MD to investigate the sliding action of polishing particles on silicon surfaces during Si CMP and reported that localized high pressure caused silicon to transform from a diamond to a metallic structure under particle sliding, leading to material removal through plastic deformation and a smooth surface finish. In summary, the sliding action refers to the relative motion of abrasive particles, whose sharp edges are held under pressure and move across the workpiece surface. This motion removes the softened surface layer or scraped reaction product films through microcutting, plowing, and scraping actions, making it the primary contributor to the MRR in CMPs.

Rolling. As illustrated in Fig. 3(d), Si et al. [122] demonstrated through MD simulations that a diamond ellipsoid confined between single-crystal silicon substrates transitions from rolling motion to sliding motion when the applied normal load exceeds 160 nN. This motion mode can be predicted by the e/h value and the friction coefficient, which determine the phase-change-driven plastic deformation and the sine wave fluctuation of frictional forces. These results offer a theoretical foundation for enhancing surface quality and process efficiency in CMPs. Subsequent MD simulations investigated three-body abrasive wear behavior in a CMP configuration consisting of a single-crystal silicon substrate,

amorphous silicon oxide clusters, and a polyurethane pad. The clusters were found to slide over smooth regions in a suspended state and roll over micro protrusions on the silicon surface, achieving damage-free removal at the atomic level [123]. The motion and interaction of abrasive particles play crucial roles in wafer planarization: particles embedded within the pad predominantly remove material through plowing mechanisms, whereas those dispersed in the slurry tend to roll along the wafer surface. Using MD simulations, the rolling process of particles over silicon protrusions was investigated under various normal and driving forces. These simulations revealed morphological changes in the protrusions and analyzed the energy evolution and interaction forces on the silica particles [124]. The simulation results demonstrated that during the rolling of abrasive particles (e.g., silica abrasives commonly used in CMP) across the silicon substrate, surface atoms undergo removal and subsequent adhesion to the abrasive surfaces, thereby creating atomic vacancies on the substrate surface—these vacancies are critical for achieving atomic-scale surface smoothness by reducing local protrusions in subsequent polishing steps [122, 124–126]. Both rolling and sliding were shown to facilitate essential atomic-scale material removal. The mechanism of atomic-scale material removal involves intricate interactions between abrasives and the substrate, especially under three-body wear conditions. Shi et al. [127] investigated the three-body wear of ellipsoidal particles on silicon under different normal pressures via MD simulations. As shown in Fig. 3(e), the transition from rolling to sliding under varying normal loads was further clarified, enhancing the understanding of particle motion processes and their significant effects on surface damage and quality. In summary, the abrasive particles roll freely as rigid spheres at the polishing interface, exerting extremely high localized contact pressure on the workpiece surface. This pressure induces microfractures or initiates and propagates microcracks in brittle materials and causes fatigue damage in ductile materials, thereby facilitating material removal.

The oxide film plays a complex and critical role in both the CMP and nanoindentation processes. Ref. [126] employed MD simulations to investigate the material removal mechanism of a crystalline silicon substrate coated with an oxide layer when impacted by silica clusters—a key scenario for oxide-mediated material removal in CMPs. An increase in oxide layer thickness revealed an optimum that maximized atomic removal from the target surface, resulting from the coupled influence of interfacial bonding—among the cluster, oxide film, and substrate—along with oxide layer coherence and the extent of atomic penetration into the substrate. Notably, the optimal oxide layer (approximately 2.5–3.0 nm thick) forms a continuous monomolecular structure. The study also revealed that the contact–penetration–adhesion (CPA) material removal process (Fig. 3(g)) occurred during CMP, which differs from traditional indentation–sliding mechanisms (Fig. 3(f)) because silicon substrate atoms penetrate the oxide layer. Chen et al. [128] integrated nanoindentation tests with MD simulations to investigate the mechanical response of single-crystal silicon coated with amorphous silica layers of different thicknesses. Their results showed that the computed indentation modulus increased with deeper penetration for both coated and uncoated silicon substrates. At a fixed indentation depth, however, the modulus decreased with increasing film thickness, a trend attributed to the diminishing contribution from the underlying silicon substrate. Indentation hardness, which is more sensitive to variations in silica film thickness, displayed nonmonotonic behavior resulting from plastic flow within the amorphous film, indicative of strain-softening mechanisms. During indentation, the amorphous silica film underwent four distinct stages of plastic deformation: densification, densification-to-fracture transition, fracture under loading, and elastic recovery during unloading. Each stage was validated by tracking variations in the silicon atom coordination number (CN) and the number of Si–O bonds with indentation depth. The study concluded that the silica thin film acts as an energy dissipation medium, effectively transmitting the indenter-applied pressure to the silicon substrate beneath. MD simulations further revealed that stress variations led to distinct phase distribution patterns in silicon materials with and without silica thin films under identical indentation depths. This oxide film functions not only as a byproduct of chemical reactions in CMP and nanoindentation but also as a mechanical transmission medium and interface modulator. Its thickness, stability, and adhesive properties significantly affect the material removal efficiency and surface quality. The identification of an optimal oxide thickness, proposal of the CPA model, and clarification of the role of the oxide layer in modulating substrate deformation provide a critical theoretical basis for understanding atomic-scale polishing mechanisms in CMPs.

The classical MD simulations discussed herein primarily elucidate the mechanical aspects of material removal and deformation, such as abrasive sliding, rolling, and the mechanical response of oxide films. However, because they rely on predefined potential functions, they are inherently limited in modeling the formation and breaking of chemical bonds. Consequently, classical MD cannot directly simulate the chemical reaction pathways involved in surface passivation during polishing or the molecular-scale cleaning mechanisms in post-CMP cleaning. This limitation naturally motivates the use of more advanced methods, such as ReaxFF and AIMD, which are introduced in the following sections to address the chemical complexities of the CMP process.

2.2 Applying ReaxFF MD to CMP & post-CMP cleaning

ReaxFF employs an empirical potential with continuously variable bond orders, effectively addressing the limitations of quantum chemistry in modeling large-scale dynamic systems and overcoming the inability of conventional force fields to accurately represent bond dissociation and formation processes [6, 7]. It expresses the bond order as a continuous function of the atomic distance, updating the atomic charges in real time. This allows the simulation of systems with up to hundreds of thousands of atoms and on ns timescales without sacrificing the accuracy of the reaction pathways. Its main advantages include modeling the continuous breaking and reformation of chemical bonds without requiring predefined reaction mechanisms; employing a unified parameter set that remains valid across solid, liquid, and gaseous states, thereby enabling its application in complex interfaces in CMPs involving abrasives, substrates, and solutions; offering computational costs 2–3 orders of magnitude lower than those of quantum chemistry, enabling simulations at the million-atom scale on GPUs or parallel CPUs; and being fully parameterized for CMP and cleaning-related systems such as C/H/O/N/Si, Cu/O/H/Cl, and Ce/O/Si, which can directly predict oxidation, adsorption, material removal, and contamination residual behaviors.

The ReaxFF reactive force field was used to address three core issues in silicon substrate CMP and postcleaning processes that have been experimentally obscured: which atomic-level bond breaking pathways dominate material removal during polishing; how the oxide layer and interfacial water work together to determine the removal rate; and how the chemical–mechanical competition between particle redeposition and desorption changes with humidity and oxidation state during the postcleaning phase.

To address these issues, Wen et al. [43] first used the Si(100)–H_2O_2–SiO_2 system as a simulation model, and their findings revealed that mechanical shear first triggers the formation of Si–O–Si bridging bonds at the interface. Subsequent to this bond formation, the Si–Si and Si–O bonds undergo continuous stretching and eventual breakage. This process explained the experimentally observed phenomenon that oxidizers significantly enhance the MRR and revealed that the increase in frictional force stems from the increased number of cycles of bond formation and breaking. Wang and Duan [129] further quantified the material removal contributions of four distinct wear mechanisms on the Si(110) surface. They emphasized that local lattice distortions resulting from oxygen atom insertion were the dominant factor in material removal, whereas the oxide layer mainly functioned as a supplier of insertable oxygen atoms rather than facilitating additional bridging bond formation. This understanding provides a theoretical basis for controlling oxidation depth. As shown in Fig. 4(a), Wen et al. [130] systematically studied the pressure effect: the number of interface bridging bonds increased linearly with load, leading to more silicon atoms being stripped away. At the same time, water molecules weaken Si–Si bonds through oxidation and block surface contact through hydrogen bond networks, indicating the dual roles of chemical promotion and mechanical inhibition. During the post-CMP cleaning process, as illustrated in Fig. 4(b), Zeng et al. [33] tracked the redeposition-removal process of 3 nm SiO_2 abrasives on the Si(100) surface and reported that increased environmental humidity formed a water buffer layer between the particles and the substrate, significantly reducing the generation of Si–O–Si and Si–Si bonds and thereby lowering the redeposition probability. However, following H_2O_2 pretreatment and subsequent oxidation of the substrate, the interfacial Si–O–Si bonds gained strength, thereby increasing the lateral shear force necessary for desorption. This implies that excessive oxidation could adversely affect cleaning performance. Finally, Wen et al. [131] provided atomic-level guidance for surface orientation selection and temperature control in CMP processes by comparing wet oxidation simulations of Si(100), (110), and (111) orientations at 300 and 500 K, supplementing the understanding of the decisive impact of crystal orientation and temperature on surface hydroxyl coverage, oxygen diffusion depth, and final oxidation state distribution.

The ReaxFF reactive force field was used in copper substrate CMP research to address three core issues that experiments cannot directly access: how the oxidizer H_2O_2 and complexing agents synergistically weaken Cu–Cu bonds and facilitate cluster removal at the atomic scale; how mechanical shear couples with surface hydroxylation/complexation reactions to reduce the desorption energy barrier of Cu atoms; and the quantitative

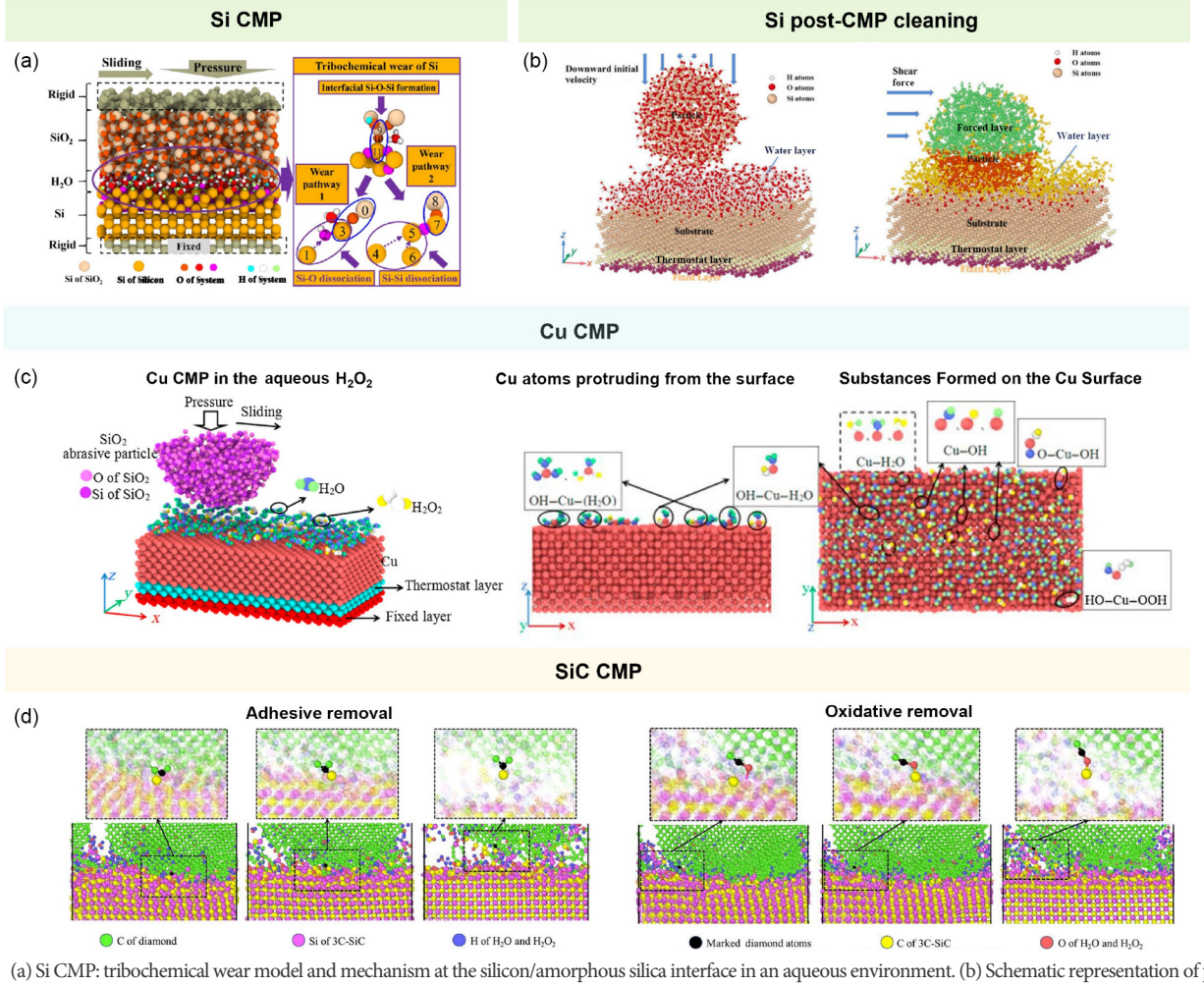

Fig. 4 (a) Si CMP: tribochemical wear model and mechanism at the silicon/amorphous silica interface in an aqueous environment. (b) Schematic representation of post-CMP cleaning mechanisms: silica nanoparticle redeposition on and removal from a silicon substrate. (c) Model illustrating copper CMP in an H_2O_2 environment, showing the copper surface prior to abrasive sliding contact. (d) Atomic adhesion mechanism in a single CMP: a comparative model schematic illustrating different polishing environments. Reproduced with permission from Ref. [130] for (a), © Elsevier B.V. 2016; Ref. [33] for (b), © Elsevier B.V. 2022; Ref. [44] for (c), © Elsevier B.V. 2018; Ref. [136] for (d), © Elsevier B.V. 2023.

correlation mechanism between the Cu atom removal efficiency and surface roughness under different slurry compositions. The ReaxFF study of copper CMP not only revealed the atomic-level removal pathways but also quantified the chemical-mechanical synergy parameters. Wen et al. [132] noted through ReaxFF MD calculations that the energy barrier for H_2O_2 dissociation on the Cu surface is only 3.0 kcal/mol, which is much lower than that of H_2O (27.9 kcal/mol), leading to the rapid generation of Cu–OH and providing active sites for subsequent bond breaking. At the same time, the adsorption energy of glycine's $-NH_2$ group with copper to form Cu–N bonds is −18.5 kcal/mol, which is stronger than that of –COOH (−6.9 kcal/mol), which causes the surface Cu atoms to protrude significantly, reducing the shear stress required for mechanical stripping. As shown in Fig. 4(c), Guo et al. [44] further reported that at a pressure of 5 GPa, 26 Cu atoms were removed, whereas only 10 were removed at 4 GPa, all from the first layer, indicating that pressure directly increases the removal rate by increasing the stretching frequency of the Cu-Cu bonds. Additionally, water molecules decompose more under high pressure, and their reduced quantity weakens lubrication, resulting in higher friction, thereby verifying the "oxidation-shear" positive feedback mechanism. Tian et al. [14] systematically varied the H_2O_2 concentration and reported that the Cu-OH ratio increased linearly with H_2O_2, but excessive oxide layer thickness suppressed the oxidation of subsurface Cu atoms as a result of brittle film formation, which consequently reduced the MRR. After the addition of glycine, the Cu-$C_2H_5O_2N$ complex promoted the continuous generation of OH free radicals, achieving peak removal efficiency with a slurry of 2.5% H_2O_2 + 0.1 M glycine. Guo et al. [40] noted that the addition of glycine not only inhibits H_2O adsorption but also induces Cu atoms to strip off as the $C_2H_5O_2N$-Cu complex via Cu-N bonds. This process is represented in the simulation by a notable increase in the number of atoms with displacements greater than 3 Å, and the experimental AFM roughness of 0.104 nm aligns closely with the simulation result of 0.082 nm, thus verifying the precise control of surface quality through slurry composition at the atomic level.

ReaxFF MD reduces the core challenges of CMP and post-CMP cleaning to the computable quantity of "the time evolution of interface atomic bond order". By tracking the formation, stretching, and breaking of chemical bonds such as C–O, Si–O, Cu–O, and Ce–O–Si in real time, macroscopic process parameters (pressure, oxidant concentration, and hydroxyl coverage) can be quantified into bond order change curves. This, in turn, predicts the MRR, removal modes (single atom/chain/lamellar), and depth of the polishing agent residue and bonding forms, providing atomic-level criteria for processing windows and cleaning endpoints. Two studies on diamond systems [45, 133] indicate that OH free radicals first react with surface C to form C–OH/C=O, weakening the neighboring C–C bonds. Mechanical sliding then stretches the bond lengths until they break, with carbon being removed in the form of CO/CO_2 or C chains. Elevated pressure enhances the adsorption of hydroxyl groups onto the surface, which correlates with a linear rise in the MRR. Quartz glass CMP simulations [134] demonstrate that both H_2O and H_2O_2 promote the generation of Si–O–Si bridging bonds connecting surface Si–OH groups and abrasive Si–O species, with the quantity of these bonds increasing as pressure increases. The removal mode involves a single atom at low hydroxyl coverage, a shift to a chain form at 30% coverage, and at 50% coverage, steric effects reduce the removal rate. In post-CMP cleaning, SiC mirror Ce contamination research [135] combining ReaxFF and experimental results confirmed that CeO_2 abrasives form Ce–O–Si bonds with the substrate, with the contamination exhibiting a 31 nm exponential decay, and that the ion beams can completely remove it. Zhou et al. [136] studied the chemical-mechanical coupling mechanism of diamond abrasive polishing of 3C-SiC via the ReaxFF-MD system. As shown in Fig. 4(d), the simulations revealed that, on the SiC surface in an H_2O_2 solution, three types of chemical adsorption primarily occur: –H, –OH, and –O–, with –OH being the most oxidative and capable of further dissociation to generate –O– bridging bonds. Three removal pathways are quantitatively differentiated: mechanical removal originates from amorphization induced by abrasives; adhesive removal occurs through direct C–Si/C–C bonding between SiC and diamond, leading to the removal of atomic clusters; and oxidative removal relies on –O– bridging bonds, which carry surface and subsurface C atoms away in the form of Si–O–C or C–O–C.

In summary, ReaxFF connects process parameters, interface bonding evolution, and macroscopic removal/residue behavior, providing an atomic-level theoretical framework for CMP optimization and subsequent cleaning. While the capabilities of ReaxFF are substantial, a balanced view necessitates acknowledging its reliance on empirically derived parameter sets. The predictive accuracy for any given system (e.g., Si/H/O, Cu/glycine, or Ce/Si) is contingent upon the quality and breadth of the training data (typically from quantum mechanics or experiments) used to optimize these parameters. Consequently, the transferability of a parameter set to chemical environments far beyond its training domain may be limited. This underscores the importance of selecting well-validated parameters and the ongoing efforts within the community to develop more robust and universal parameter sets.

2.3 Applying TB-QC MD to CMPs and post-CMP cleaning

TB-QC MD couples the quantum description of chemical bonds with classical nuclear motion within the same framework, allowing long-term tracking of large-scale interfaces without sacrificing crucial electronic effects. The method starts with the extended Hückel tight-binding approximation, constructing a nondiagonal Hamiltonian via the distance-dependent Wolfsberg–Helmholtz equation, and calibrates the ionization energy of each element's valence orbitals and Slater exponent via first-principles calculations. This keeps the bond length prediction error of Cu–O, Si–O, and similar bonds within 0.05 Å. The system's total energy is augmented with long-range Coulombic and short-range repulsive contributions derived from the summation of electronic eigenvalues. Concurrently, the analytical force expression incorporates gradients of both the Hamiltonian and overlap matrices, thereby ensuring conservation of energy and stability of the dynamical trajectory. Compared with CPMD, the TB-QC MD method lowers the computational expense by approximately 1,000 times, allowing real-time monitoring of bond populations, atomic charge distributions, and orbital occupancies for systems consisting of several hundred atoms over time scales of hundreds of ps. This allows the inclusion of charge transfer and bond order changes, which traditional classical MD neglects, in the simultaneous description of friction-chemical reactions. Typically, TB-QC MD enables simulations of systems comprising several hundred atoms for hundreds of picoseconds, positioning it as a balanced approach that bridges the gap between the quantum accuracy but limited scale of AIMD (~100 atoms, ~ps) and the larger scale but empirical parameter dependence of ReaxFF (~100,000 atoms, ~ns).

In the typical force-chemical coupling process of CMP, TB-QC MD integrates the three elements of "slurry chemistry, surface reactions, and abrasive mechanics" into a unified atomic-level

framework. The flowchart corresponding to the "Colors" program and the critical optimization measures for CMP processes are illustrated in Fig. 5(a) [137]. For the silica system [137, 138], when the abrasive is silica, its molecular model is shown in Fig. 5(b), demonstrating substantial shifts in the electronic states of the silicon surface. When the abrasive is CeO_2, the CeO_2 abrasives can break the Si–O bonds of SiO_2 and form Si–O–Ce bridging bonds within 600–1,000 fs of sliding, accompanied by electron transfer from Ce^{4+} to Ce^{3+}. This explains the high selectivity of cerium-containing slurries. The models are illustrated in Fig. 5(c). On hydrogen-terminated Si(100) surfaces, abrasive sliding induces the gradual desorption of H atoms, generating Si–OH. The bond occupancy decreases sharply from 2.896 to 2.311, indicating surface electronic state instability, thus improving the material removal efficiency. Additionally, the simulation shows that the slurry pH influences the dissociation equilibrium of H_2O_2, thereby altering the depth of oxidation. Neutral conditions are favorable for generating a passivation layer of controllable thickness, whereas strongly acidic environments lead to excessive corrosion. A quintessential example that underscores the power of TB-QC MD is its application to the peroxide-driven CMP of a copper surface [46, 139]. The simulation explicitly modeled the dissociation of H_2O_2 on a Cu(111) surface under the mechanical shear of a sliding abrasive (as depicted in Figs. 5(d) and 5(e)). The simulation captured the atomistic process in real time: H_2O_2 first dissociates into adsorbed OH and O species, but critically, these oxygen atoms do not spontaneously embed into the copper lattice. The key insight emerged when the localized shear stress from the abrasive actively drove the adsorbed oxygen atoms into the subsurface layer, a step identified to have a high energy barrier of 28 kcal/mol. This observation directly revealed that the "mechanical force trigger" is the rate-determining step in the material removal process, as thermal energy alone at room temperature is insufficient to overcome this barrier. Following this mechanical activation, the weakened Cu–Cu bonds break, leading to the formation of protruding atoms that are eventually removed as $Cu(OH)_2$ clusters. Compared with Cu(100), Cu(111) more readily forms a stable Cu_2O/CuO passivation layer on the surface, thereby suppressing excessive oxidation and pit formation, providing quantitative guidance for the selection of process parameters on the basis of the crystal plane orientation. TB-QC MD thus transforms the empirical "oxidation–mechanical removal" cycle into a computable energy–charge–stress trajectory, laying the atomic-scale theoretical foundation for the rational design of slurry formulations, abrasive materials, and process parameters.

A critical question arises when comparing the ReaxFF MD and TB-QC MD results for Cu CMP: what are their distinct advantages, and how do they complement each other? While both methods successfully simulate bond formation/dissociation and estimate energy barriers, the nature of their insights differs significantly owing to their underlying philosophies.

ReaxFF MD, parameterized against empirical or quantum data, offers a high-fidelity dynamic narrative. Its lower computational cost allows for the simulation of larger systems (thousands of atoms) over longer timescales, capturing the complete sequence of events—from H_2O_2 adsorption and dissociation to the mechanically driven insertion of oxygen and finally the detachment of Cu complexes. It excels at showing how a reaction pathway unfolds in time and under a mechanical stimulus. TB-

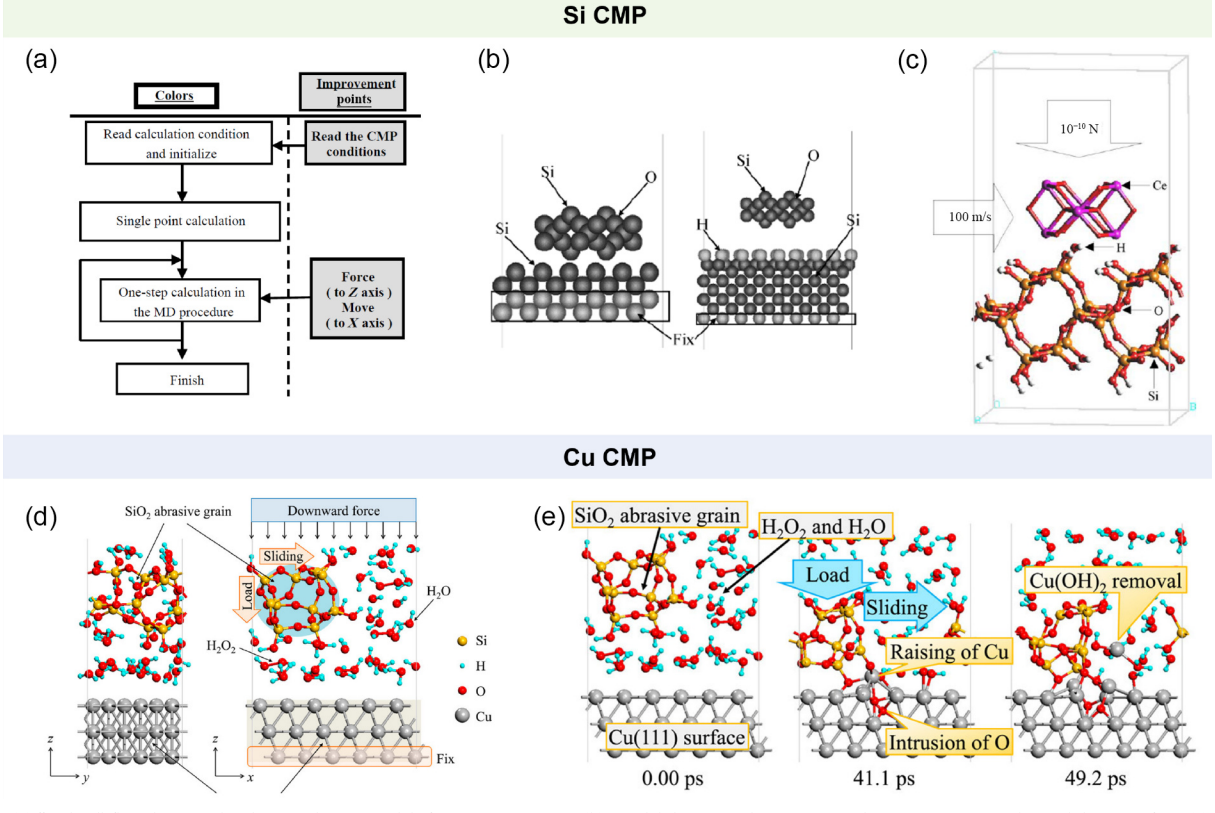

Fig. 5 (a) "Colors" flowchart: molecular simulation models for CMP processes. (b) Model depicting the interaction between SiO_2 particles and the Si surface. (c) Model depicting the interaction between CeO_2 particles and the SiO_2 surface. Models for the Cu CMP process: (d) model involving SiO_2 particles and water molecules; (e) model of peroxide molecules interacting with the copper substrate surface. Reproduced with permission from Ref. [137] for (a, b), © The Japan Society of Applied Physics 2002; Ref. [138] for (c), © Elsevier B.V. 2004; Ref. [46] for (d, e), © American Chemical Society 2016.

QC MD, grounded in a quantum-chemical framework, provides electronic-level mechanistic insight. Although it is applied to smaller systems for shorter durations, its primary strength lies in directly computing electronic properties. It can quantify charge transfer during bond formation (e.g., electron transfer between Cu and adsorbates) and trace the evolution of orbital occupancies, thereby revealing why a specific reaction step has a particular energy barrier. The energy barrier of 28 kcal/mol for oxygen insertion obtained from TB-QC MD, for example, comes with a higher degree of quantum-mechanical credibility for the specific system it was calibrated for.

In essence, they form a powerful complementary pair: ReaxFF MD acts as a "computational story-teller", which is ideal for exploring and visualizing plausible full reaction pathways and their dynamic coupling with mechanics. TB-QC MD, in contrast, serves as a "computational analyst" used to validate and gain deep electronic insight into the key transition states or reaction steps identified by ReaxFF MD. Together, they provide a multifaceted understanding that is greater than the sum of their parts, bridging the gap between observable dynamics and the underlying quantum mechanical driving forces in CMP processes.

2.4 Applying the AIMD to CMP & post-CMP cleaning

Classical MD employs predefined empirical potentials, such as the Lennard–Jones potential, to model atomic interactions. While this approach is computationally efficient, it tends to be inaccurate for covalent or metallic bond systems and cannot provide electronic structure information. On the other hand, electronic structure calculations via DFT can accurately describe chemical bonds, but their enormous computational cost—due to the repeated solving of the KS equations—limits their application in large systems, disordered systems, and MD simulations that require atomic forces to be calculated. The innovation of Car and Perriello was the proposal of a unified framework that seamlessly integrates MD with DFT. Their method introduces fictitious dynamics to describe electronic degrees of freedom (KS orbitals), allowing them to evolve in parallel with real ionic dynamics under the same extended Lagrangian framework. This breakthrough enabled MD simulations at DFT accuracy, directly calculating atomic forces on the basis of quantum mechanics without relying on empirical potentials. It also allows for the efficient optimization of the ground-state electronic structure and geometric structure of large systems, including lattice constants, strain, and atomic positions. The equations of motion derived from the Lagrangian method are as Eqs. (18)–(20):

$$\mu\ddot{\psi}_i(r,t) = -\frac{\delta E}{\delta \psi_i^*(r,t)} + \sum_k \Lambda_{ik}\psi_k(r,t) \tag{18}$$

$$M_I\ddot{R}_I = -\nabla_{R_I}E \tag{19}$$

$$\mu_\nu\ddot{\alpha}_\nu = -\frac{\partial E}{\partial \alpha_\nu} \tag{20}$$

Equation (18) describes the dynamics of this motion. The first term on the right, $-\frac{\delta E}{\delta \psi_i^*(r,t)}$, serves as the driving force for motion. It is proportional to the derivative of the energy increment with respect to the current state of the KS equations. The second term, ψ_i, is an initial estimate of the single-particle wave function. Clearly, this process involves repeated iterations of the KS setup, demonstrating how one updates the approximation ϵ_i for KS calculations in a certain way. Equation (19) describes the dynamics of its true state. $-\nabla_{R_I}E$ is a complex term generated by some type of expectation value. This arises from the Hellmann–Feynman theorem and is determined by the current wave function.

The system evolves through the numerical integration of the motion in Eq. (7). Initially, a "temperature" (i.e., initial kinetic energy) is assigned to the electronic orbits. The evolution of the entire system can be viewed as a form of dynamic simulated annealing. If the positions of the ions are fixed (or they are slowly moved) while gradually lowering the system's "temperature" (through velocity scaling or other thermostats), the kinetic energy of the electronic orbits gradually decreases. When the temperature $T\to 0$, the system relaxes to the minimum point of the KS energy functional, corresponding to the ground state electronic structure, while concurrently optimizing the ion positions and the unit cell. At this point, Eq. (19) provides the correct KS orbitals and eigenvalues. Moreover, while keeping the electrons in or very close to their instantaneous ground state, the ions are allowed to move according to the forces calculated from quantum mechanics with their true physical mass MIMI. This requires that the "kinetic energy" of the electronic orbits be very small, meaning that the "motion" of the electronic orbits is extremely slow. This implies that the system remains within a very thin layer of the Born–Oppenheimer (BO) potential energy surface, with "thickness" measured by the effective temperature corresponding to the electronic degrees of freedom. By selecting an appropriate fictitious mass and integration time steps, the total energy of the electrons closely follows the motion of the ions while remaining near the instantaneous ground state while ensuring numerical stability. At this point, the ion trajectory described by Eq. (20) approximately represents the real physical dynamics obtained from classical MD simulations on the DFT potential energy surface. This method has been successfully applied to calculate the static properties of crystalline silicon (such as energy bands and lattice constant optimization) and the dynamic properties (including the excitation and evolution of specific phonon modes and their frequencies). It addresses the dynamic behavior at finite temperatures and is, in principle, applicable to any system that can be described by DFT, including solids, liquids, surfaces, molecules, and clusters.

A study [140] dedicated to the tribochemical mechanism at the CeO_2/SiO_2 interface employed CPMD simulations, revealing for the first time the atomic-level mechanisms of SiO_2 surface polishing by CeO_2 abrasives in an aqueous setting. The study constructed a sliding interface model involving hydrogen-terminated silicon dioxide surfaces and $H_4Ce_6O_{12}$ clusters, explicitly including 72 water molecules to simulate the slurry environment (see Fig. 6(a)). Under a normal load of 50 pN/atom and a shear force of 500 pN/atom, the simulations revealed that friction induced the formation of Ce–O–Si bridging bonds at the interface. This subsequently triggered the creation of a second bridging bond, which converted the silicon atom into an unstable five-coordinated intermediate; the mechanism of bond breaking was identified, whereby five-coordinated silicon achieved surface flattening by breaking the original Si–O bond, a process reliant on the cooperative effect of multiple Ce–O–Si bonds; crucially, it was established that under dry friction conditions (without water molecules), even with the formation of Ce–O–Si bonds, breaking the Si–O bond is difficult, confirming that water molecules weaken the Si–O bond through adsorption. Furthermore, as shown in Fig. 6(b), the effects of the CeO_2 (100) and (111) crystal planes were compared, revealing that the (111) facet could form five-coordinate silicon and trigger bond breaking because its hexagonal adsorption sites facilitate the formation of key

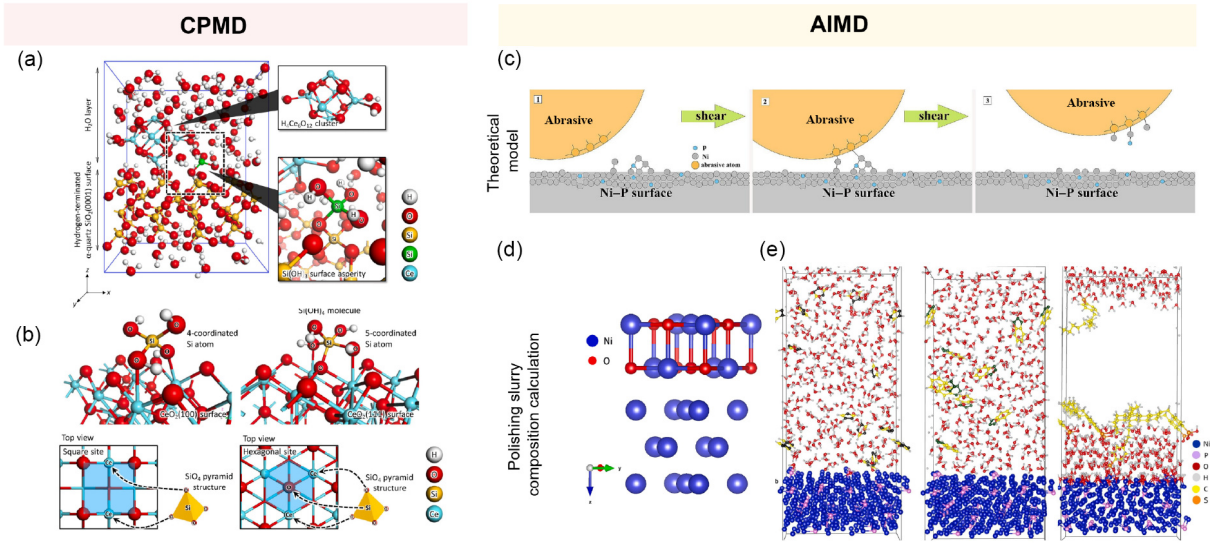

Fig. 6 (a) MD simulation setup for analyzing tribochemical reaction kinetics at a ceria–silica sliding interface. (b) Configurations of $Si(OH)_4$ chemically adsorbed on ceria surfaces with varying crystallographic orientations optimized via CPMD. (c) Schematic of the material removal mechanism for a single atom/layer of Ni-P. (d) Structural model depicting two NiO layers adhered to a substrate of Ni atoms. (e) Computational simulation outcomes for BTA, TAZ, and DBSA inhibitors. Reproduced with permission from Ref. [140] for (a, b), © Elsevier B.V. 2020; Ref. [140] for (c–e), © Elsevier B.V. 2025.

intermediates, whereas the square sites of the (100) plane were ineffective. Through CPMD, this research elucidated the atomic pathway of "multibridging bond-induced bond breaking" in CMPs, providing a theoretical basis for the design of efficient polishing slurries.

Wang et al. [141] integrated AIMD simulations with DFT calculations to elucidate the atomic-scale material removal mechanisms during the CMP of Ni-P alloys—an essential process for semiconductor interconnect fabrication—thereby providing guidance for the rational design of slurries tailored to alloy substrates. One of the key findings is the establishment of a removal model grounded in the "chemical tooth" theory, indicating that SiO_2 abrasives remove Ni-P surface atoms through three mechanisms: the adsorption of O atoms on isolated Ni atoms, which is the dominant mechanism; the stripping of P atoms after O bonds with P, due to the stronger Si-O-P bond than the Ni-P bond; and the synergistic detachment of O-P-Ni from the surface, as shown in Fig. 6(c). For slurry component optimization, the DFT calculations of binding energies demonstrated that the binding energy of SiO_2 with Ni_3P (−13.328 eV) is significantly greater than that of α-Al_2O_3 (−1.904 eV), leading to the selection of SiO_2 as the abrasive. Furthermore, as shown in Fig. 6(d), AIMD simulations revealed that, compared with BTA, SDS/SLS adsorbs more effectively on the Ni-P surface, helping to prevent excessive corrosion. This research confirms that AIMD and DFT can precisely guide slurry development, enabling the manufacture of atomically smooth surfaces.

The application of AIMD to the study of CMP and post-CMP cleaning remains relatively limited, yet its potential for illuminating atomic-scale mechanisms is immense. It is crucial to recognize the inherent spatiotemporal boundaries of AIMD simulations to properly contextualize their findings. Typical AIMD studies, as highlighted in the cases above, handle systems on the scale of tens to a few hundred atoms over durations of tens of picoseconds. This scale is not suitable for simulating an entire polishing process. Instead, the unparalleled value of AIMD lies in its ability to act as a "computational microscope", capturing the precise bond-breaking/forming steps, reaction pathways, and short-range interactions that are fundamental to the tribochemical process. The insights derived—such as the identification of a rate-determining step or the role of a specific surface facet—are thus mechanistic in nature. They provide the foundational chemical understanding, which can then inform larger-scale models or guide the interpretation of macroscopic experiments. Given its capacity to precisely depict chemical processes, AIMD holds significant potential for expanding its applications to address more specialized and complex challenges in CMP and beyond.

3 Challenges and future directions

3.1 Multiscale modeling

Multiscale coupling achieves cross-scale information transfer via real-time or dynamic integration of models at different scales. Its core lies in overcoming the limitations of single-scale models and capturing interactions spanning from the microscopic to the macroscopic levels. For example, in materials science, the bonding characteristics at the quantum scale may directly influence the macroscopic mechanical properties of a material. The simulation methods used in multiscale simulations include quantum chemistry calculations, atomistic MD, kinetic MC simulations or coarse-grained MC, and computational fluid dynamics. Quantum chemistry methods can be used at the atomic scale, and the simulation time can reach ps. The atomistic MD simulation can reach the nm dimensional scale, and the time scale can reach the ns level. The MC simulation and computational fluid dynamics are relatively high. However, it seems unreasonable to directly incorporate atomic information such as force conditions at the continuum level.

MC simulation, alternatively referred to as the statistical simulation method, is a numerical calculation approach rooted in probability statistics. It simulates complex systems or processes through random sampling and statistical experiments and is especially well suited for analyzing complex problems such as uncertainty, probability distribution models, and high-dimensional integrals. In this case, the information of the atomistic scale can only be transferred to this method by sequential coupling. Fortunately, the data at the atomistic level can serve as input information for the upper scale through sequential coupling. This method has already been implemented in another

research area [142–144]. There are several studies on MC simulations of the CMP process; however, they do not directly consider information at the atomistic scale [145–147]. Borucki et al. [145] developed statistical models to demonstrate the change in pad surface roughness throughout the pad-conditioning stage of CMP processes. These proposed models describe the temporal changes in the surface height probability density function of solid conditioning pads under operational conditions with fixed heights and fixed cut rates. Chen et al. [146] established a modified MC approach with a new objective for the multilayer fill problem. Moreover, Kong et al. [147] constructed a process performance prediction model—capable of estimating indicators such as MRR—by integrating statistical regression analysis and a nonlinear Bayesian method. A promising direction for future research would be to develop an MC model that simulates bond formation and breakage processes during CMP.

3.2 AIMD

To develop linear scaling DFT methods and accelerate quantum computing techniques to reduce computational complexity, we combine (graphics processing unit-GPU/tensor processing unit-TPU) heterogeneous computing with a quantum computing architecture to achieve real-time simulations of million atom-level systems [91, 148]. AIMD can directly describe electron–atom interactions and can accurately simulate the polishing process [149, 150]. Noninquilibrium ab initio molecular dynamics (NEAIMD), rooted in quantum mechanics, offers a transformative framework to elucidate atomic-scale mechanisms by directly simulating electron ion dynamics during CMP. NEAIMD can be employed to investigate the coupling of the external shear force and chemical kinetics. Modeling the effect of local temperature increases on surface oxidation kinetics. Using a hybrid quantum-classical approach, quantum calculations are performed only in the reaction area.

3.3 Potential functions

The calculation accuracy of MD depends on the accuracy of the potential function. The parameters of the classical force potential are obtained via artificial fit experimental or quantum chemical data. This limits its ability to describe multicomponent systems (such as high-entropy alloys), complex chemical interactions (such as bond breakage and formation), and quantum effects (such as polarization and charge transfer). To address these problems, potential methods based on deep neural networks or machine learning could be developed. Recent advancements in machine-learned force fields have transitioned from demonstrating conceptual feasibility to addressing specific scientific and engineering challenges, showing significant progress in both methodological innovation and practical applications. Potential functions based on deep neural networks (such as D and anisotropic neural network potential-ANI) have achieved orders of magnitude acceleration under DFT accuracy, pushing AIMD to the microsecond time scale [151, 152]. On the methodological front, Zhang et al. [151] proposed an adaptive scheme that couples a DeePMD model with a classical force field. This approach partitions the simulation system into high-accuracy regions described by DeePMD, highly efficient regions governed by a classical force field, and transition regions between them. By employing force interpolation and imposing a thermodynamic force, the high-accuracy region is seamlessly embedded within a large-scale simulation environment. The successful validation of this method in a water system demonstrates that such multiscale approaches provide a powerful computational framework for simulating processes such as CMP, which inherently involve both atomistic chemical reactions at interfaces and macroscopic transport in the bulk medium. In terms of material applications, Sun et al. [152] developed a neural network potential for the Fe–Si alloy system, demonstrating the ability of MLFFs to handle complex materials. This potential accurately describes the structures and energies of various crystalline phases and liquids across a wide composition range from Fe-rich to Si-rich and reveals the competition between amorphization and crystallization during rapid solidification. This study proves the ability of MLFFs to capture mixed metallic and covalent bonding accurately in metal–semiconductor systems, which is highly relevant for understanding the complex interfacial interactions between abrasives and wafers (e.g., silicon, copper, and silica) in CMPs. Collectively, these advancements indicate that machine-learned force fields are evolving into a key enabling technology for driving material design, including the optimization of CMP processes.

4 Conclusions

In summary, this review highlights the critical role of CMP and post-CMP cleaning in semiconductor manufacturing. By focusing on the application of MD simulations, we identify how different methodologies—classical MD, ReaxFF, TB-QC MD, and AIMD—contribute to understanding the atomic-scale mechanisms involved in these processes. Each method offers unique advantages: classical MD allows large-scale simulations, whereas ReaxFF provides insights into chemical reactions during polishing. TB-QC MD integrates quantum accuracy with classical efficiency, and AIMD captures detailed atomic interactions. This diverse approach enables a more comprehensive understanding of material removal mechanisms and contaminant dynamics. However, the broader adoption of these simulations is often constrained by challenges in force field parameterization for complex chemical environments and the need for further experimental validation to confirm predictive accuracy. Future research should prioritize addressing the challenges associated with multiscale modeling and seek to increase the efficiency of AIMD. Furthermore, the development of precise potential functions is essential for accurately modeling complex chemical interactions. By pursuing these avenues, researchers can further advance the optimization of CMP processes, ultimately improving the performance and reliability of semiconductor devices.

Acknowledgements

This work was financially supported by the National Natural Science Foundation of China (Grant No. 51991370). The authors acknowledge the support of the Tsinghua University Initiative Scientific Research Program.

Declaration of competing interest

The authors have no competing interests to declare that are relevant to the content of this article.

References

[1] Lorenz J, Bär E, Barraud S, Brown A R, Evanschitzky P, Klüpfel F, Wang L P. Process variability: Technological challenge and design issue for nanoscale devices. *Micromachines* **10**(1): 6 (2019)

[2] Dong C, Liu Y, Han T Y, Zhou X, Meng Y N, Tian Y, Ma, L R. Effect of hydrated ions and wettability on ice friction. *Friction* **13**(7): 9440972 (2025)

[3] Moore G E. Cramming more components onto integrated circuits. *Proc IEEE* **86**(1): 82–85 (1998)

[4] Van Gunsteren W F, Oostenbrink C. Methods for classical-

mechanical molecular simulation in chemistry: Achievements, limitations, perspectives. *J Chem Inf Model* **64**(16): 6281–6304 (2024)

[5] Zhou J K, Niu X H, Liu Z L, Ma Q, Li J H, Hu B, Wu Z. Revolutionizing chemical mechanical polishing with machine learning: A comprehensive review of challenges and opportunities. *Arch Comput Meth Eng* **33**(1): 823–857 (2026)

[6] Senftle T P, Hong S, Islam M M, Kylasa S B, Zheng Y X, Shin Y K, Junkermeier C, Engel-Herbert R, Janik M J, Aktulga H M, et al. The ReaxFF reactive force-field: Development, applications and future directions. *npj Comput Mater* **2**: 15011 (2016)

[7] Chen Y S, Jiang L, Qian L M. AFM probe for measuring ~10^{-5} ultra-low friction coefficient: Design and application. *Friction* **12**(1): 64–73 (2024)

[8] Zhou M F, Zhong M, Xu W H. Novel model of material removal rate on ultrasonic-assisted chemical mechanical polishing for sapphire. *Friction* **11**(11): 2073–2090 (2023)

[9] Banerjee G, Rhoades R L. Chemical mechanical planarization historical review and future direction. *ECS Trans* **13**(4): 1–19 (2008)

[10] Hisamoto D, Lee W C, Kedzierski J, Takeuchi H, Asano K, Kuo C, Anderson E, King T J, Bokor J, Hu C M. FinFET—A self-aligned double-gate MOSFET scalable to 20 nm. *IEEE Trans Electron Devices* **47**(12): 2320–2325 (2000)

[11] Zhang L F, Zhao N H, Ci H, Zhao D W, Lu X C. Slurry injection schemes based on flow field distribution during chemical mechanical polishing process. *Friction* https://doi.org/10.26599/FRICT.2025.9441185 (2025)

[12] Arima K, Kubota A, Mimura H, Inagaki K, Endo K, Mori Y, Yamauchi K. Highly resolved scanning tunneling microscopy study of Si(001) surfaces flattened in aqueous environment. *Surf Sci* **600**(15): 185–188 (2006)

[13] Chen L, Wen J L, Zhang P, Yu B J, Chen C, Ma T B, Lu X C, Kim S H, Qian L M. Nanomanufacturing of silicon surface with a single atomic layer precision via mechanochemical reactions. *Nat Commun* **9**: 1542 (2018)

[14] Tian Z Q, Wang S Z, Li R, Sun X, Shen W, Liu S. Study on polishing mechanisms of BEOL metal interconnects based on chemical and mechanical synergy. *Microsyst Nanoeng* **11**: 109 (2025)

[15] Qing Z L, Sun C Q, Li Z L, Li Z M. Unlocking the potential of CMP synthesis: Merging enzyme design, host genome editing, and fermentation optimization strategy. *Process Biochem* **149**: 204–212 (2025)

[16] Di Y Q, Pan G F, Lv S, She L N, Zhai L, Qi Y H. Chemical mechanical polishing on cobalt-based barrier through dual functionality of salicylhydroxamic acid between the removal of copper and corrosion inhibition. *Electrochim Acta* **514**: 145689 (2025)

[17] Krishnan M, Nalaskowski J W, Cook L M. Chemical mechanical planarization: Slurry chemistry, materials, and mechanisms. *Chem Rev* **110**(1): 178–204 (2010)

[18] Sahir S, Cho H W, Kim T G, Hamada S, Yerriboina N P, Park J G. Study on PVA brush loading and conditioning during shallow trench isolation post-CMP cleaning process. *ECS J Solid State Sci Technol* **11**(2): 024004 (2022)

[19] Zhang L F, Xie L L, Lu X C. Effect of ionic surfactants on shallow trench isolation for chemical mechanical polishing using ceria-based slurries. *Cogent Eng* **10**(2): 2272354 (2023)

[20] Zhang L F, Xie L L, Lu X C. Enhancing ceria slurry performance for shallow trench isolation chemical mechanical polishing through non-ionic surfactant addition. *Int J Adv Manuf Technol* **128**(11–12): 4997–5010 (2023)

[21] Dai H F, Yue H X, Hu Y, Li P. The removal mechanism of monocrystalline Si in the process of double diamond abrasive polishing by molecular dynamics simulation. *Tribol Lett* **69**(2): 66 (2021)

[22] Johnson C A, Roy D. Editors' choice: in situ electrochemical evaluation of post-CMP cleaning reactions for cobalt and copper films under brushing conditions. *ECS J Solid State Sci Technol* **8**(5): P3163–P3174 (2019)

[23] Thompson A P, Aktulga H M, Berger R, Bolintineanu D S, Brown W M, Crozier P S, in'T Veld P J, Kohlmeyer A, Moore S G, Nguyen T D, et al. LAMMPS—A flexible simulation tool for particle-based materials modeling at the atomic, meso, and continuum scales. *Comput Phys Commu* **271**: 108171 (2022)

[24] Xu Y X, Wang M C, Zhu F L, Liu X J, Liu Y H, He L P. Study on subsurface damage of wafer silicon containing through silicon via in thinning. *Eur Phys J Plus* **134**(5): 234 (2019)

[25] Cheng Y S, Wang S L, Li H L, Wang C W, Yang Y D, Lei S S, Li S. Study on particle removal during the Co post-CMP cleaning process. *Colloids Surf A Physicochem Eng Aspects* **627**: 127189 (2021)

[26] Kim I-K, Nagendra Prasad Y, Kwon T-Y, Kim H-M, Busnaina A A, Park J-G. Citric acid and $NaIO_4$ based alkaline cleaning solution for particle removal during post-Ru CMP cleaning. *J Electrochem Soc* **158**(10): 52 (2011)

[27] Song J, Park K, Jeon S, Lee J, Kim T. Development of a novel wet cleaning solution for post-CMP SiO_2 and Si_3N_4 films. *Mat Sci in Semicon Proc* **140**: 106353 (2022)

[28] Cui H X, Ma T D, Tan B M, Sun X Q, Feng Z X. Unraveling the mechanism of removing NA contamination by TMAH-based cleaning solution during post co-CMP cleaning. *ECS J Solid State Sci Technol* **11**(3): 034005 (2022)

[29] Liu P Z, Hong S, Jeon S, Lee J, Kwak D, Wada Y, Hiyama H, Hamada S, Kim T. Investigations on the mechanism of silica particle removal during the Cu buff cleaning process. *Colloids Surf A Physicochem Eng Aspects* **627**: 127156 (2021)

[30] Zhang L F, Wang T Q, Nan J P, Lu X C. Developing an efficient forward design method for co post-CMP cleaning formulations based on nanoparticle removal mechanisms. *ACS Appl Electron Mater* **5**(12): 6884–6896 (2023)

[31] Zhang S H, Wang Y Z, Tan B M, Wang F Y, Wang X L, Du H Y. Experimental characterization and dynamical modeling evaluation for enhanced BTA removal by three amino acids in post-Cu-CMP cleaning. *J Mol Liq* **382**: 121987 (2023)

[32] Thompson S E, Parthasarathy S. Moore's law: The future of Si microelectronics. *Mater Today* **9**(6): 20–25 (2006)

[33] Zeng Q Y, Li C K, Zhao D W, Lu X C. Atomic-scale study on particle movement mechanism during silicon substrate cleaning using ReaxFF MD. *Comput Mater Sci* **214**: 111751 (2022)

[34] Chen S D, Lei H. Improvement in the planarization of 4H-SiC(0001) achieved by photo-assisted chemical mechanical polishing (P-CMP) using nano TiO_2-based composite abrasive with heterostructure. *Friction* **13**(7): 9440993 (2025)

[35] Shi X L, Chen G P, Xu L, Kang C X, Luo G H, Luo H M, Zhou Y, Dargusch M S, Pan G S. Achieving ultralow surface roughness and high material removal rate in fused silica via a novel acid SiO_2 slurry and its chemical-mechanical polishing mechanism. *Appl Surf Sci* **500**: 144041 (2020)

[36] Xu Q Z, Chen L, Yang F, Cao H. Influence of slurry components on copper CMP performance in alkaline slurry. *Microelectron Eng* **183–184**: 1–11 (2017)

[37] Du T B, Vijayakumar A, Desai V. Effect of hydrogen peroxide on oxidation of copper in CMP slurries containing glycine and Cu ions. *Electrochim Acta* **49**(25): 4505–4512 (2004)

[38] Han X Y, Zhang S H, Liu R H, Wang F Y, Tan B M, Zhao X Y, Zhao J D, Shi Y H. The effect of amino acid addition in CeO_2-based slurry on SiO_2/Si_3N_4 CMP: Removal rate selectivity, morphology, and mechanism research. *J Mol Liq* **412**: 125855 (2024)

[39] Srivastava I, Kotia A, Ghosh S K, Ali M K A. Recent advances of molecular dynamics simulations in nanotribology. *J Mol Liq* **335**: 116154 (2021)

[40] Guo X G, Yuan S, Gou Y J, Wang X L, Guo J, Jin Z J, Kang R K. Study on chemical effects of H_2O_2 and glycine in the copper CMP process using ReaxFF MD. *Appl Surf Sci* **508**: 145262 (2020)

[41] Wu Y, Jiang L, Li W H, Zheng J X, Chen Y S, Qian L M. Two material removal modes in chemical mechanical polishing:

Mechanical plowing vs. chemical bonding. *Friction* **12**(5): 897–905 (2024)
[42] Morishita T, Kayanuma M, Nakamura T, Kato T. Cooperative reaction of hydrogen-networked water molecules at the SiC–H_2O_2 solution interface: Microscopic insights from ab initio molecular dynamics. *J Phys Chem C* **126**(30): 12441–12449 (2022)
[43] Wen J L, Ma T B, Zhang W W, van Duin A C T, Lu X C. Atomistic mechanisms of Si chemical mechanical polishing in aqueous H_2O_2: ReaxFF reactive molecular dynamics simulations. *Comput Mater Sci* **131**: 230–238 (2017)
[44] Guo X G, Wang X L, Jin Z J, Kang R K. Atomistic mechanisms of Cu CMP in aqueous H_2O_2: Molecular dynamics simulations using ReaxFF reactive force field. *Comput Mater Sci* **155**: 476–482 (2018)
[45] Guo X G, Yuan S, Wang X L, Jin Z J, Kang R K. Atomistic mechanisms of chemical mechanical polishing of diamond (100) in aqueous H_2O_2/pure H_2O: Molecular dynamics simulations using reactive force field (ReaxFF). *Comput Mater Sci* **157**: 99–106 (2019)
[46] Kawaguchi K, Ito H, Kuwahara T, Higuchi Y, Ozawa N, Kubo M. Atomistic mechanisms of chemical mechanical polishing of a Cu surface in aqueous H_2O_2: Tight-binding quantum chemical molecular dynamics simulations. *ACS Appl Mater Interfaces* **8**(18): 11830–11841 (2016)
[47] Zhang S Q, Liu Y R, Li W M, Cao J, Huang J Y, Zhu L, Guan Z J. Numerical analysis of the effect of retaining ring structure on the chemical mechanical polishing abrasive motion state. *Materials* **16**(1): 62 (2023)
[48] Srinivasa-Murthy C, Wang D, Beaudoin S P, Bibby T, Holland K, Cale T S. Stress distribution in chemical mechanical polishing. *Thin Solid Films* **308**: 533–537 (1997)
[49] Wang T Q, Lu X C. Numerical and experimental investigation on multi-zone chemical mechanical planarization. *Microelectron Eng* **88**(11): 3327–3332 (2011)
[50] Liu P Z, Kang C, Oh S, Jeon S, Lee H, Wang Z Y, Jeong H, Lee E, Kim T. Investigating the impact of pad groove depth reduction on process variation in oxide chemical mechanical polishing. *ECS J Solid State Sci Technol* **13**(10): 104006 (2024)
[51] Cho Y, Liu P Z, Jeon S, Lee J, Bae S, Hong S, Kim Y H, Kim T. Simulation and experimental investigation of the radial groove effect on slurry flow in oxide chemical mechanical polishing. *Appl Sci* **12**(9): 4339 (2022)
[52] Bozkaya D, Muftu S. A material removal model for CMP based on the contact mechanics of pad, abrasives, and wafer. *J Electrochem Soc* **156**(12): H890 (2009)
[53] Preston F W. The theory and design of plate glass polishing machines. *J Soc Glass Tech* **11**: 214–256 (1927)
[54] Maury A, Ouma D O, Boning D S, Chung J E. A modification to Preston's equation and impact on pattern density effect modeling. In: Proceedings of Advanced Metallization Conference, 1997.
[55] Tseng W T, Wang Y L. Re-examination of pressure and speed dependences of removal rate during chemical–mechanical polishing processes. *J Electrochem Soc* **144**(2): L15 (1997)
[56] Shi F G, Zhao B. Modeling of chemical–mechanical polishing with soft pads. *Appl Phys A Mater Sci Process* **67**(2): 249–252 (1998)
[57] Liu C W, Dai B T, Tseng W T, Yeh C F. Modeling of the wear mechanism during chemical–mechanical polishing. *J Electrochem Soc* **143**(2): 716–721 (1996)
[58] Luo J F, Dornfeld D A. Material removal mechanism in chemical mechanical polishing: Theory and modeling. *IEEE Trans Semicond Manuf* **14**(2): 112–133 (2001)
[59] Zhao Y W, Chang L. A micro-contact and wear model for chemical–mechanical polishing of silicon wafers. *Wear* **252**(3–4): 220–226 (2002)
[60] Zhao Y W, Chang L, Kim S H. A mathematical model for chemical–mechanical polishing based on formation and removal of weakly bonded molecular species. *Wear* **254**(3–4): 332–339 (2003)
[61] Jeng Y R, Wang P Y. An elliptical microcontact model considering elastic, elastoplastic, and plastic deformation. *J Tribol* **125**(2): 232–240 (2003)
[62] Jeng Y R, Huang P Y. A material removal rate model considering interfacial micro-contact wear behavior for chemical mechanical polishing. *J Tribol* **127**(1): 190–197 (2005)
[63] Wang Y G, Chen Y, Qi F, Zhao D, Liu W W. A material removal model for silicon oxide layers in chemical mechanical planarization considering the promoted chemical reaction by the down pressure. *Tribol Int* **93**: 11–16 (2016)
[64] Zhao D W, Lu X C. Chemical mechanical polishing: Theory and experiment. *Friction* **1**(4): 306–326 (2013)
[65] Kim H, Jeong H. Effect of process conditions on uniformity of velocity and wear distance of pad and wafer during chemical mechanical planarization. *Journal Elec Materi* **33**(1): 53–60 (2004)
[66] Beverina A. Copper photocorrosion phenomenon during post CMP cleaning. *Electrochem Solid-State Lett* **3**(3): 156 (1999)
[67] Nishi A, Sado M, Miki T, Fukui Y. Evaluation of the Cu-CMP process by TOF-SIMS and XPS: Time dependence of Cu surface adsorbents and oxidation states. *Appl Surf Sci* **203**: 470–472 (2003)
[68] Lo B, Tai C C, Chang J, Wu C, Chen B, Kuo T C, Lian P J, Ling Y. Supercritical carbon dioxide-assisted oxidative degradation and removal of polymer residue after reactive ion etching of photoresist. *Green Chem* **9**(2): 133–138 (2007)
[69] Fernando W J N, Lok Y H, Don M M, Madhaven V, Tay W S. Experimental and modeling studies of particle removal in post silicon chemical mechanical planarization cleaning process. *Thin Solid Films* **519**(10): 3242–3248 (2011)
[70] Krishnan M, Lofaro M F. Copper chemical mechanical planarization (Cu CMP) challenges in 22 nm back-end-of-line (BEOL) and beyond. In: *Advances in Chemical Mechanical Planarization (CMP)*. Babu S, Ed. Amsterdam (the Netherlands): Elsevier, 2016: 27–46.
[71] Chen C, Xiao C, Wang X D, Zhang P, Chen L, Qi Y Q, Qian L M. Role of water in the tribochemical removal of bare silicon. *Appl Surf Sci* **390**: 696–702 (2016)
[72] Lim D S, Ahn J W, Park H S, Shin J H. The effect of CeO_2 abrasive size on dishing and step height reduction of silicon oxide film in STI–CMP. *Surf Coat Technol* **200**(5–6): 1751–1754 (2005)
[73] Heyns M M, Verhaverbeke S, Meuris M, Mertens P W, Schmidt H, Kubota M, Philipossian A, Dellenbeck K, Gräf D, Schnegg A, et al. New wet cleaning strategies for obtaining highly reliable thin oxides. *MRS Online Proc Libr* **315**(1): 35–45 (1993)
[74] Yang X M, Zhong Z W, Diallo E M, Wang Z H, Yue W S. Silicon wafer wettability and aging behaviors: Impact on gold thin-film morphology. *Mater Sci Semicond Process* **26**: 25–32 (2014)
[75] Zhang F, Busnaina A A, Ahmadi G. Particle adhesion and removal in chemical mechanical polishing and post-CMP cleaning. *J Electrochem Soc* **146**(7): 2665–2669 (1999)
[76] Sun T, Han Z X, Keswani M. Brush scrubbing for post-CMP cleaning. In: *Developments in Surface Contamination and Cleaning*. Kohli R, Mittal K L, Eds. Amsterdam (the Netherlands): Elsevier, 2017: 109–133.
[77] Rahman A. Correlations in the motion of atoms in liquid argon. *Phys Rev* **136**(2A): A405–A411 (1964)
[78] Xu W H, Sheng C, Zhong M. Effects of ultrasonic vibration on sapphire polishing investigated by molecular dynamics. *Tribol Int* **176**: 107911 (2022)
[79] Wei B Y, Kong N, Zhang J, Li H B, Hong Z J, Zhu H T, Zhuang Y, Wang B. A molecular dynamics study on the tribological behavior of molybdenum disulfide with grain boundary defects during scratching processes. *Friction* **9**(5): 1198–1212 (2021)
[80] Figueira F L, Van Steenberge P H M, Zhou Y N, Luo Z H, D'hooge D R. Macromolecular kinetic Monte Carlo simulations taking only a moment. *Chem Eng J* **521**: 166229 (2025)
[81] Mi W H, Luo K, Trickey S B, Pavanello M. Orbital-free density functional theory: An attractive electronic structure method for large-scale first-principles simulations. *Chem Rev* **123**(21): 12039–12104 (2023)
[82] Lin K, Wang Z L. Multiscale mechanics and molecular dynamics

simulations of the durability of fiber-reinforced polymer composites. *Commun Mater* **4**: 66 (2023)
[83] De Keer L, Kilic K I, Van Steenberge P H M, Daelemans L, Kodura D, Frisch H, De Clerck K, Reyniers M F, Barner-Kowollik C, Dauskardt R H, et al. Computational prediction of the molecular configuration of three-dimensional network polymers. *Nat Mater* **20**(10): 1422–1430 (2021)
[84] Liu H G, Xu X, Zhang J, Liu Z C, He Y, Zhao W H, Liu Z Q. The state of the art for numerical simulations of the effect of the microstructure and its evolution in the metal-cutting processes. *Int J Mach Tools Manuf* **177**: 103890 (2022)
[85] Stephan S, Schmitt S, Hasse H, Urbassek H M. Molecular dynamics simulation of the Stribeck curve: Boundary lubrication, mixed lubrication, and hydrodynamic lubrication on the atomistic level. *Friction* **11**(12): 2342–2366 (2023)
[86] Yuan S, Guo X G, Wang H, Kang R K, Gao S. Atomistic understanding of rough surface on the interfacial friction behavior during the chemical mechanical polishing process of diamond. *Friction* **12**(6): 1119–1132 (2024)
[87] Visser J. On Hamaker constants: A comparison between Hamaker constants and Lifshitz-van der Waals constants. *Adv Colloid Interface Sci* **3**(4): 331–363 (1972)
[88] Hamaker H C. The London—van der Waals attraction between spherical particles. *Physica* **4**(10): 1058–1072 (1937)
[89] Case D A, Cheatham T E III, Darden T, Gohlke H, Luo R, Merz K M Jr, Onufriev A, Simmerling C, Wang B, Woods R J. The Amber biomolecular simulation programs. *J Comput Chem* **26**(16): 1668–1688 (2005)
[90] Hwang W, Austin S L, Blondel A, Boittier E D, Boresch S, Buck M, Buckner J, Caflisch A, Chang H T, Cheng X, et al. CHARMM at 45: Enhancements in accessibility, functionality, and speed. *J Phys Chem B* **128**(41): 9976–10042 (2024)
[91] Allec S I, Sun Y J, Sun J N, Chang C A, Wong B M. Heterogeneous CPU+GPU-enabled simulations for DFTB molecular dynamics of large chemical and biological systems. *J Chem Theory Comput* **15**(5): 2807–2815 (2019)
[92] Phillips J C, Hardy D J, Maia J D C, Stone J E, Ribeiro J V, Bernardi R C, Buch R, Fiorin G, Hénin J, Jiang W, et al. Scalable molecular dynamics on CPU and GPU architectures with NAMD. *J Chem Phys* **153**(4): 044130 (2020)
[93] Todorov I T, Smith W, Trachenko K, Dove M T. DL_POLY$_3$: New dimensions in molecular dynamics simulations via massive parallelism. *J Mater Chem* **16**(20): 1911 (2006)
[94] Gale J D, Rohl A L. The general utility lattice program (GULP). *Mol Simul* **29**(5): 291–341 (2003)
[95] Li Q, Cheng B, Chen M Y, Xie B, Xie Y Q, Wang P F, Chen F Q, Liu Z L, Watanabe K, Taniguchi T, et al. Tunable quantum criticalities in an isospin extended Hubbard model simulator. *Nature* **609** (7927): 479–484 (2022)
[96] Zhou M F, Zhong M, Xu W H. Effects of ultrasonic amplitude on sapphire ultrasonic vibration assisted chemical mechanical polishing by experimental and CFD method. *Mech Adv Mater Struct* **29**(28): 7086–7103 (2022)
[97] Cheng J, Wang T Q, He Y Y, Lu X C. Material removal mechanism of copper chemical mechanical polishing in a periodate-based slurry. *Appl Surf Sci* **337**: 130–137 (2015)
[98] Perdew J P, Burke K, Ernzerhof M. Generalized gradient approximation made simple. *Phys Rev Lett* **77**(18): 3865–3868 (1996)
[99] Agrawal P M, Raff L M, Bukkapatnam S, Komanduri R. Molecular dynamics investigations on polishing of a silicon wafer with a diamond abrasive. *Appl Phys A* **100**(1): 89–104 (2010)
[100] Goedecker S. Linear scaling electronic structure methods. *Rev Mod Phys* **71**(4): 1085–1123 (1999)
[101] Shi P F, Yin Y, Zhang S H, Zhang D K, Jiang Y Y, Wang Y, Zhou N N, Qing T, Wu J T, Qian L M, et al. Blackening failure of poly-α-olefin impregnated porous polymide due to the splitting of lubrication oil catalyzed by iron. *Friction* **12**(9): 1969–1979 (2024)
[102] Tang Y J, Zheng M, Ren C X, Li X X, Guo L. Visualized reaction tracking and physical property analysis for a picked 3D area in a reactive molecular dynamics simulation system. *Acta Phys Chim Sin* **37**(10): 2003037 (2021)
[103] Zhang L F, Zeng Q Y, Huang Y T, Zhao D W, Xiao Y Q, Fu Z M. Atomic-scale study on nanoparticle removal mechanism during post-Cu CMP cleaning process using ReaxFF MD. *Appl Surf Sci* **717**: 164864 (2026)
[104] Allen M P, Tildesley D J. *Computer Simulation of Liquids*. Oxford University Press, 2017.
[105] Tuckerman M E. Ab initio molecular dynamics: Basic concepts, current trends and novel applications. *J Phys: Condens Matter* **14**(50): R1297–R1355 (2002)
[106] Wang X J, Xiao H Y, Zu X T, Zhang Y, Weber W J. Ab initio molecular dynamics simulations of ion–solid interactions in $Gd_2Zr_2O_7$ and $Gd_2Ti_2O_7$. *J Mater Chem C* **1**(8): 1665 (2013)
[107] Yang Z D, Wang X, Li Y F, Lv Q J, Chen C Y, Shen L. Efficient equivariant model for machine learning interatomic potentials. *npj Comput Mater* **11**: 49 (2025)
[108] Mathieu D, Borges I. Molecular dynamics simulation of hot spot formation and chemical reactions. In: *Theoretical and Computational Chemistry*. Mathieu D, Ed. Elsevier, 2022: 255–289.
[109] Rimsza J M, Yeon J, van Duin A C T, Du J C. Water interactions with nanoporous silica: Comparison of ReaxFF and ab initio based molecular dynamics simulations. *J Phys Chem C* **120**(43): 24803–24816 (2016)
[110] Van Duin A C T, Dasgupta S, Lorant F, Goddard W A. ReaxFF: A reactive force field for hydrocarbons. *J Phys Chem A* **105**(41): 9396–9409 (2001)
[111] Chenoweth K, van Duin A C T, Goddard W A. ReaxFF reactive force field for molecular dynamics simulations of hydrocarbon oxidation. *J Phys Chem A* **112**(5): 1040–1053 (2008)
[112] Stillinger F H, Weber T A. Computer simulation of local order in condensed phases of silicon. *Phys Rev B* **31**(8): 5262–5271 (1985)
[113] Tersoff J. New empirical model for the structural properties of silicon. *Phys Rev Lett* **56**(6): 632–635 (1986)
[114] Car R, Parrinello M. Unified approach for molecular dynamics and density-functional theory. *Phys Rev Lett* **55**(22): 2471–2474 (1985)
[115] Kumar K, Xu J Q, Wu G, Verma A, Mishra A K, Gao L, Ogata S. Recent trends and progress in molecular dynamics simulations of 2D materials for tribological applications: An extensive review. *Arch Computat Methods Eng* **32**(6): 3909–3931 (2025)
[116] Chen R L, Luo J B, Guo D, Lu X C. Extrusion formation mechanism on silicon surface under the silica cluster impact studied by molecular dynamics simulation. *J Appl Phys* **104**(10): 104907 (2008)
[117] Chen R L, Jiang R R, Lei H, Liang M. Material removal mechanism during porous silica cluster impact on crystal silicon substrate studied by molecular dynamics simulation. *Appl Surf Sci* **264**: 148–156 (2013)
[118] Shi J Q, Chen J, Fang L, Sun K, Sun J P, Han J. Atomistic scale nanoscratching behavior of monocrystalline Cu influenced by water film in CMP process. *Appl Surf Sci* **435**: 983–992 (2018)
[119] Ye Y, Biswas R, Bastawros A, Chandra A. Simulation of chemical mechanical planarization of copper with molecular dynamics. *Appl Phys Lett* **81**(10): 1875–1877 (2002)
[120] Dai H F, Yue H X, Hu Y, Li P. The removal mechanism of monocrystalline Si in the process of double diamond abrasive polishing by molecular dynamics simulation. *Tribol Lett* **69**: 66 (2021)
[121] Han X S, Hu Y Z, Yu S Y. Investigation of material removal mechanism of silicon wafer in the chemical mechanical polishing process using molecular dynamics simulation method. *Appl Phys A* **95**(3): 899–905 (2009)
[122] Si L N, Guo D, Luo J B, Lu X C, Xie G X. Abrasive rolling effects on material removal and surface finish in chemical mechanical polishing analyzed by molecular dynamics simulation. *J Appl Phys* **109**(8): 084335 (2011)

[123] Chen R L, Li S X. Novel three-body nano-abrasive wear mechanism. *Friction* **10**(5): 677–687 (2022)
[124] Si L N, Guo D, Luo J B, Xie G X. Planarization process of single crystalline silicon asperity under abrasive rolling effect studied by molecular dynamics simulation. *Appl Phys A* **109**(1): 119–126 (2012)
[125] Chen R L, Zhou P J, Li H. Effect of rotation of abrasives on material removal in chemical mechanical polishing using a proposed three-body model: Molecular dynamics simulation. *Tribol Int* **196**: 109716 (2024)
[126] Chen R L, Wu Y H, Lei H, Jiang R R, Liang M. Study of material removal processes of the crystal silicon substrate covered by an oxide film under a silica cluster impact: Molecular dynamics simulation. *Appl Surf Sci* **305**: 609–616 (2014)
[127] Shi J Q, Chen J, Wei X Q, Fang L, Sun K, Sun J P, Han J. Influence of normal load on the three-body abrasion behaviour of monocrystalline silicon with ellipsoidal particle. *RSC Adv* **7**(49): 30929–30940 (2017)
[128] Chen J, Shi J Q, Chen Z, Zhang M, Peng W X, Fang L, Sun K, Han J. Mechanical properties and deformation behaviors of surface-modified silicon: A molecular dynamics study. *J Mater Sci* **54**(4): 3096–3110 (2019)
[129] Wang M, Duan F L. Atomic-level material removal mechanisms of Si(110) chemical mechanical polishing: Insights from ReaxFF reactive molecular dynamics simulations. *Langmuir* **37**(6): 2161–2169 (2021)
[130] Wen J L, Ma T B, Zhang W W, Psofogiannakis G, van Duin A C T, Chen L, Qian L M, Hu Y Z, Lu X C. Atomic insight into tribochemical wear mechanism of silicon at the Si/SiO_2 interface in aqueous environment: Molecular dynamics simulations using ReaxFF reactive force field. *Appl Surf Sci* **390**: 216–223 (2016)
[131] Wen J L, Ma T B, Zhang W W, van Duin A C T, Lu X C. Surface orientation and temperature effects on the interaction of silicon with water: Molecular dynamics simulations using ReaxFF reactive force field. *J Phys Chem A* **121**(3): 587–594 (2017)
[132] Wen J L, Ma T B, Zhang W W, van Duin A C T, van Duin D M, Hu Y Z, Lu X C. Atomistic insights into Cu chemical mechanical polishing mechanism in aqueous hydrogen peroxide and glycine: ReaxFF reactive molecular dynamics simulations. *J Phys Chem C* **123**(43): 26467–26474 (2019)
[133] Shi Z Y, Jin Z J, Guo X G, Yuan S, Guo J. Insights into the atomistic behavior in diamond chemical mechanical polishing with OH environment using ReaxFF molecular dynamics simulation. *Comput Mater Sci* **166**: 136–142 (2019)
[134] Guo X G, Yuan S, Huang J X, Chen C, Kang R K, Jin Z J, Guo D M. Effects of pressure and slurry on removal mechanism during the chemical mechanical polishing of quartz glass using ReaxFF MD. *Appl Surf Sci* **505**: 144610 (2020)
[135] Li Y J, Li L X, Wei H D, Li X C, Wang Y R, Pan S, Zhang X J. Cerium contamination on silicon carbide optics during CMP: TOF-SIMS, XPS characterization, and ReaxFF MD simulation. *Appl Surf Sci* **703**: 163390 (2025)
[136] Zhou Y Q, Huang Y H, Li J M, Lv W S, Zhu F L. Investigation of the chemical action mechanism based on reactive force field in SiC chemical–mechanical polishing process. *Appl Surf Sci* **646**: 158927 (2024)
[137] Yokosuka T, Kurokawa H, Takami S, Kubo M, Miyamoto A, Imamura A. Development of new tight-binding molecular dynamics program to simulate chemical-mechanical polishing processes. *Jpn J Appl Phys* **41**(Part 1, No. 4B): 2410–2413 (2002)
[138] Rajendran A, Takahashi Y, Koyama M, Kubo M, Miyamoto A. Tight-binding quantum chemical molecular dynamics simulation of mechano-chemical reactions during chemical–mechanical polishing process of SiO_2 surface by CeO_2 particle. *Appl Surf Sci* **244**(1–4): 34–38 (2005)
[139] Yokosuka T, Sasata K, Kurokawa H, Takami S, Kubo M, Imamura A, Miyamoto A. Quantum chemical molecular dynamics studies on the chemical mechanical polishing process of Cu surface. *Jpn J Appl Phys* **42**(4S): 1897 (2003)
[140] Onodera T, Takahashi H, Nomura S. First-principles molecular dynamics investigation of ceria/silica sliding interface toward functional materials design for chemical mechanical polishing process. *Appl Surf Sci* **530**: 147259 (2020)
[141] Wang Y X, Yang C, Bai Y, Wang X, Xu G, Sun X L, Zou C S. Atomic-level removal mechanism study of nickel-phosphorus (Ni–P) alloy based on AIMD and DFT calculation. *Appl Surf Sci* **709**: 163816 (2025)
[142] Kabir M, Lau T T, Rodney D, Yip S, Van Vliet K J. Predicting dislocation climb and creep from explicit atomistic details. *Phys Rev Lett* **105**(9): 095501 (2010)
[143] Stoller R E, Golubov S I, Domain C, Becquart C S. Mean field rate theory and object kinetic Monte Carlo: A comparison of kinetic models. *J Nucl Mater* **382**(2–3): 77–90 (2008)
[144] Goswami K N, Mottura A. A kinetic Monte Carlo study of vacancy diffusion in non-dilute Ni–Re alloys. *Mater Sci Eng A* **743**: 265–273 (2019)
[145] Borucki L J, Witelski T, Please C, Kramer P R, Schwendeman D. A theory of pad conditioning for chemical-mechanical polishing. *J Eng Math* **50**(1): 5266160 (2004)
[146] Chen Y, Kahng A B, Robins G, Zelikovsky A. Monte-Carlo methods for chemical–mechanical planarization on multiple-layer and dual-material models. *Des Process Integr Charact Microelectron* **4692**: 421–432 (2002)
[147] Kong Z Y, Oztekin A, Beyca O F, Phatak U, Bukkapatnam S T S, Komanduri R. Process performance prediction for chemical mechanical planarization (CMP) by integration of nonlinear Bayesian analysis and statistical modeling. *IEEE Trans Semicond Manuf* **23**(2): 316–327 (2010)
[148] Kohn W. Density functional theory for systems of very many atoms. *Int J Quantum Chem* **56**(4): 229–232 (1995)
[149] Du Y T, Yang F C, Guo Z G. Interfacial mechanical and tribochemical effects on friction mechanisms under air or vacuum conditions. *Friction* **13**(12): 9441056 (2025)
[150] He X J, Yu T T, Wu Z S, Du C H, Deng H Y, Zhao Y K, Li S, Feng Y G, Zhang L Q, Zhang Z N, et al. Atomically thin MoS_2 with ultra-low friction properties based on strong interface interaction. *Friction* **13**(4): 9440936 (2025)
[151] Zhang L F, Wang H, Weinan E. Adaptive coupling of a deep neural network potential to a classical force field. *J Chem Phys* **149**(15): 154107 (2018)
[152] Sun H J, Zhang C, Tang L, Wang R H, Xia W Y, Wang C Z. Molecular dynamics simulation of Fe–Si alloys using a neural network machine learning potential. *Phys Rev B* **107**(22): 224301 (2023)

Lifei Zhang received her Ph.D. degree in Department of Mechanical Engineering from Tsinghua University, China. Her current position is an assistant professor in Tsinghua University. Her research areas cover micro/nano fabrication tribology, nano/atomic precision surface manufacturing, and chemical mechanical planarization technology.

Xinchun Lu is a professor in Tsinghua University. His research areas cover micro/nano fabrication tribology, nano/atomic precision surface manufacturing, and chemical mechanical planarization technology.